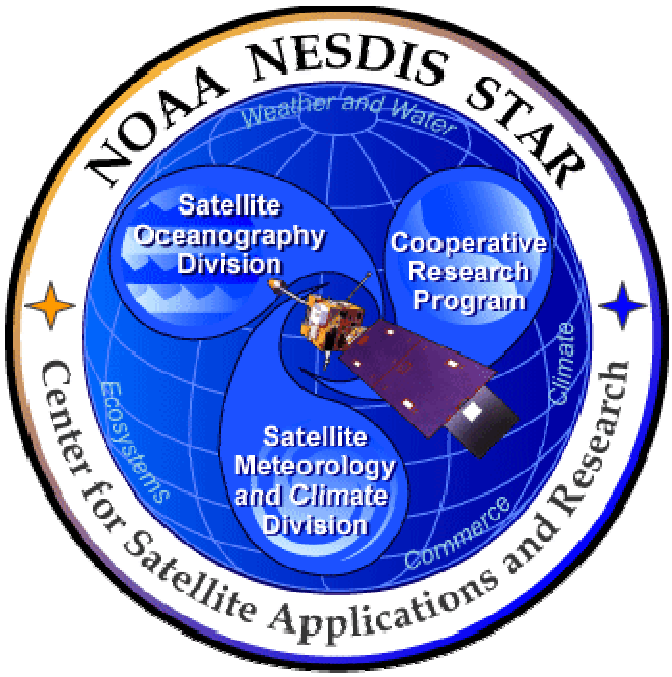


**NOAA NESDIS**
**CENTER for SATELLITE APPLICATIONS and RESEARCH**

**ALGORITHM THEORETICAL BASIS DOCUMENT**

# ABI Aerosol Detection Product

NOAA/NESDIS/STAR

Version 2.0
September 30, 2010

# TABLE OF CONTENTS

# LIST OF TABLES

# LIST OF FIGURES

# LIST OF ACRONYMS

| Acronym | Description |
|---|---|
| AAA | Aerosol, Air Quality and Atmospheric Chemistry |
| ABI | Advanced Baseline Imager |
| AIT | Algorithm Integration Team |
| ADP | Aerosol Detection Product |
| AOD | Aerosol Optical Depth |
| ATBD | Algorithm Theoretical Basis Document |
| ATIP | Algorithm and Test Implementation Plan |
| AVHRR | Advanced Very High Resolution Radiometer |
| AWG | Algorithm Working Group |
| CALIPSO | Cloud-Aerosol Lidar and Infrared Pathfinder Satellite Observation |
| CONUS | CONtiguous United States |
| BT | Brightness Temperature |
| BTD | Brightness Temperature Difference |
| FMW | Fine Mode Weight |
| F&PS | Functional and Performance Specification Document |
| GOES | Geostationary Operational Environmental Satellite |
| HMS | Hazard Mapping System |
| IMS | Interactive Multisensor Snow and Ice Mapping System |
| MeanR | Mean of reflectance (in a box of 3 X 3 pixels) |
| MODIS | Moderate Resolution Imaging Spectroradiometer |
| MRD | Mission Requirements Document |
| NDVI | Normalized Difference Vegetation Index |
| NOAA | National Wateric and Atmospheric Administration |
| R | Reflectance |
| RTM | Radiative Transfer Model |
| SST | Sea Surface Temperature |
| StdR | Standard Deviation of Reflectance (in a box of 3 X 3 pixels) |
| TOA | Top of the Atmosphere |

## ABSTRACT

This document describes the algorithm for Aerosol (including smoke/dust) Detection Product (ADP) over land and water from the multispectral reflectance measurements observed by the Advanced Baseline Imager (ABI) onboard GOES-R. It includes the description of theoretical basis, physics of the problem, validation of the product, and assumptions and limitations.

Episodic events, such as smoke and dust outbreaks, impact human health and economy. Therefore, it is desirable to have qualitative information on the time, location and coverage of these outbreaks for the monitoring and forecasting of air quality. GOES-R ABI is designed to observe the Americas in a 5-minute interval and at 0.5, 1, 2 km spatial resolution in the visible, near-IR, and IR bands respectively. Taking advantage of the unique capability of GOES-R ABI, ADP will be produced with an algorithm designed to take advantage of various spectral measurements.

Aerosol detection algorithm is based on the fact that smoke/dust exhibits features of spectral dependence and contrast over both visible and infrared spectrum that are different from clouds, surface, and clear-sky atmosphere. The fundamental principle of the detection algorithm depends on threshold tests which separate smoke/dust from cloud and clear-sky over water and land.

By using MODIS observations as proxy, GOES-R ABI smoke/dust algorithm has been tested for different scenarios such as wild fires, dust storms, and dust transport from Africa. Comparisons with RGB images and other satellite products such as CALIPSO have been performed along with a sensitivity study of the detection on the accuracy of sensor radiances/brightness temperature. In general, the requirement, i.e., 80% correct detection for dust over water and land, for smoke over land, and 70% correct detection for smoke over water, can be achieved. Preliminary analysis shows that radiometric or calibration errors at the 5% level can be tolerated.

# 1 INTRODUCTION

Aerosols perturb the Earth's energy budget by scattering and absorbing radiation and by altering cloud properties and lifetimes. They also exert large influences on weather, air quality, hydrological cycles, and ecosystems. Aerosols released into the atmosphere due to natural and anthropogenic activities lead to deteriorated air quality and affect Earth's climate. It is important to regularly monitor the global aerosol distributions and study how they are changing, especially for those aerosols with large spatial and temporal variability, such as smoke, sand storms, and dust [IPCC, 2007]. Detection of these highly variable aerosols is challenging because of strong interactions with local surface and meteorological conditions.

Because atmospheric aerosols can directly alter solar and Earth radiation in both visible and infrared (IR) spectral regions through scattering and absorption processes, both visible and IR remote sensing techniques have been used for detection of aerosols in the atmosphere [e.g., Tanre and Legrand, 1991; Ackerman 1989, 1997; Kaufman et al., 1997; Verge-Depre et al., 2006]. Visible and IR images can be used for detecting episodic smoke and dust particles due to the fact that these aerosol particles display some spectral variations in visible and IR spectral regions different from those of cloud or clear-sky conditions. In practice, the detection is based on the analysis of reflectance (or radiance) in visible bands or brightness temperature (BT) in IR bands. The magnitude of the difference in reflectance or BTs in selected bands (or channels) can be used to infer the signature of dust and smoke. This is the basic idea of our aerosol detection algorithm, which will be described in detail in this document.

## 1.1 Purpose of This Document

The aerosol detection Algorithm Theoretical Basis Document (ATBD) provides a high level description of and the physical basis for the detection of smoke/dust contaminated pixels with images taken by the Advanced Baseline Imager (ABI) flown on the GOES-R series of next generation NOAA operational geostationary meteorological satellites. The algorithm provides an initial estimate of the presence or absence of smoke or dust within each ABI pixel.

## 1.2 Who Should Use This Document

The intended users of this document are those interested in understanding the physical basis of the algorithms and how to use the output of this algorithm to optimize the episodic aerosol detection for a particular application. This document also provides information useful to anyone maintaining or modifying the original algorithm.

## 1.3 Inside Each Section

This document is broken down into the following main sections.

- **System Overview**: Provides relevant details on ABI instrument characteristics and detailed description of the products generated by the algorithm.

- **Algorithm Description**: Provides the detailed description of the algorithm including physical basis, the required input and the derived output. Examples from algorithm processing using proxy input data are also provided.

- **Test Data Sets and Outputs**: Provides a description of the test data sets used to characterize the performance of the algorithm and the quality of the output. Precision and accuracy of the end product is estimated and Error budget is calculated.

- **Practical Considerations**: Provides an overview of the issues involving numerical computation, programming and procedures, quality assessment and diagnostics and exception handling.

- **Assumptions and Limitations**: Provides an overview of assumptions which the algorithm is based on and the current limitations of the approach. The plan for overcoming some limitations with further algorithm development is also given.

## 1.4 Related Documents

Besides the references given throughout, this document is related to documents listed as bellow:

(1) GOES-R Mission Requirements Document (MRD)
(2) GOES-R Functional and Performance Specification Document (F&PS)
(3) GOSE-R ABI Aerosol Detection Product Algorithm and Test Implementation Plan (ATIP) Document
(4) GOSE-R ABI Aerosol Detection Product Validation Plan Document

## 1.5 Revision History

This is the second version (Version 2.0) of this document for 100% maturity delivery. Version 2.0 is based on Version 1.0 including not only the revisions but also improvement of algorithm itself and related changes to precision and accuracy estimates etc. All the documents were created by the GOES-R AAA ADP team led by Dr. Shobha Kondragunta of NOAA/NESDIS/STAR. The ADP team includes Dr. Steven Ackerman of University of Wisconsin-Madison and Dr. Pubu Ciren of PSGS QSS Group, Inc., Maryland. Version 2.0 ATBD accompanies the delivery of the version 5.0 algorithm to the GOES-R AWG Algorithm Integration Team (AIT).

# 2 OBSERVING SYSTEM OVERVIEW

This section will describe the products generated by the ABI ADP algorithm including smoke and dust and the requirements it places on the sensor.

## 2.1 Products Generated

As described in Tables 1 and 2, ADP measurement accuracy is defined as 80% of correct classification for dust over water and land, for smoke over land, and 70% correct classification for smoke over water with measurement range given as binary yes/no detection above threshold of 0.2 aerosol optical depth, as stated in GOES-R Ground Segment Functional and Performance Specification (F&PS) (G417-R-FPS-0089 V1.9). It should be noted that aerosol optical depth of 0.2 defines background atmospheric aerosol and is not computed with this algorithm.

**Table 1 GOES-R mission requirements for Aerosol Detection**

| Name | User & Priority | Geographic Coverage (G, H, C, M) | Vertical Res. | Horiz. Res. | Mapping Accuracy | Msmnt. Range | Msmnt. Accuracy | Refresh Rate/Coverage Time Option | Vendor-Allocated Ground Latency | Product Measurement Precision |
|---|---|---|---|---|---|---|---|---|---|---|
| Aerosol Detection (including Smoke and Dust) | GOES-R | C | Total Column | 2 km | 1 km | Binary yes/no detection above threshold 0.2 (for AOT) | Dust: 80% correct detection over land and water Smoke: 80% correct detection over land and 70% over water | 15 min | 15 min | N/A |
| Aerosol Detection (including Smoke and Dust) | GOES-R | FD | Total Column | 2 km | 1 km | Binary yes/no detection above threshold 0.2 (for AOT) | Dust: 80% correct detection over land and water Smoke: 80% correct detection over land and 70% over | 15 min | 806 sec | N/A |
| Aerosol Detection (including Smoke and Dust) | GOES-R | M | Total Column | 2 km | 1 km | Binary yes/no detection above threshold 0.2 (for AOT) | Dust: 80% correct detection over land and water Smoke: 80% correct detection over land and 70% over water | 15 min | 806 sec | N/A |

C=CONUS, FD=full disk, M= Mesoscale

**Table 2 GOES-R qualifier for Aerosol Detection**

| Name | User & Priority | Geographic Coverage (G, H, C, M) | Temporal Coverage Qualifiers | Product Extent Qualifier | Cloud Cover Conditions Qualifier | Product Statistics Qualifier |
|---|---|---|---|---|---|---|
| Aerosol Detection (including Smoke and Dust) | GOES-R | C | Day | Quantitative out to at least 60 degrees LZA and qualitative at larger LZA | Clear Conditions down to feature of interest associated with threshold accuracy | Over specified geographic area |
| Aerosol Detection (including Smoke and Dust) | GOES-R | FD | Day | Quantitative out to at least 60 degrees LZA and qualitative at larger LZA | Clear Conditions down to feature of interest associated with threshold accuracy | Over specified geographic area |
| Aerosol Detection (including Smoke and Dust) | GOES-R | M | Day | Quantitative out to at least 60 degrees LZA and qualitative at larger LZA | Clear Conditions down to feature of interest associated with threshold accuracy | Over specified geographic area |

C=CONUS, FD=full disk, M= Mesoscale

The purpose of the ADP algorithm is to identify ABI pixels which are contaminated by either smoke or dust during daytime to facilitate the monitoring of occurrences and development of smoke/dust episodes. However, due to the relatively weak contribution of aerosols compared to reflection from the surface to the satellite measured reflectances/brightness temperatures, the ADP algorithm performs better for heavy smoke /dust episodes (with aerosol optical depth >0.2) over dark surface than over bright surfaces. Smoke detection over semi-arid and arid regions is less accurate due to lower contrast with the background. The algorithm output is currently written in netCDF4 format for smoke flag (1/0 for yes/no), dust flag (1/0 for yes/no) and 4 quality flags

(contained in a 1 byte integer), i.e., smoke detection quality flag (1/0 for not determined (bad)/ determined (good), Dust detection quality flag (1/0 for not determined(bad)/ determined(good)), smoke detection confidence flag (00/01/11 for lower/medium/high confidence) and dust detection confidence flag (00/01/11 for lower/medium/high confidence). In addition, product quality information flags (contained in a 4 byte integer) are also generated but only as internal output. The details on both quality flags and product quality information flags are given in tables 3 and 4 respectively.

## 2.2 Instrument Characteristics

The ADP will be produced for each pixel observed by the ABI. Table 5 summarizes the channels used by the current ADP algorithm.

The backbone of the ADP algorithm is the distinctive spectral and spatial signature of aerosol (smoke/dust). Temporal variability has not been taken advantage of, in the current version of algorithm, but is planned for future versions. Similar to clouds, variability of smoke or dust plume is much larger than the surface over a course of day. Besides the threshold test, by tracking the variability over time, for example, variability over a course of 30 minutes, it is possible to define if a pixel is laden with smoke/dust. However, it must be noted that cloud, smoke and dust may have similar temporal variability. Taking advantage of temporal variability in smoke/dust detection has high requirement on separating clouds from smoke/dust. In addition, as shown in Table 5, different ABI channels have different spatial resolution, ranging from 0.5 km for visible to 2 km for IR channels. In ADP algorithm, the output resolution is 2km. Hence, channels with higher spatial resolution than 2 km have to be aggregated to 2km by sub-sampling before applying the ADP algorithm. Like any other threshold-based algorithm, the ADP algorithm requires optimal performance of the instrument. First, the ADP algorithm is designed to work when only a sub-set of the expected channels are available. Missing channels, especially the crucial ones, will impact directly the performance of the algorithm.

Second, the ADP algorithm is sensitive to instrument noise and calibration error. Thresholds are required to be adjusted accordingly to the status of instrument operation and performance. Third, calibrated observations are also critical, but since the algorithm does not compare the observed values to those from a forward radiative transfer model, uncertainties in calibration can be ameliorated by modifying thresholds post launch of the ABI. The channel specifications are given in the MRD.

**Table 3 Quality flags for ABI aerosol detection product**

| Byte/Bit* | | Quality Flag Name | Meaning | | |
|---|---|---|---|---|---|
| | | | 1bit: 0 (default) | 1 | |
| | | | 2bit: 00 (default) | 01 | 11 |
| 1 | 0 | QC_SMOKE_DETECTION | Determined (good) | not Determined(bad) | |
| | 1 | QC_DUST_DETECTION | Determined(good) | not Determined(bad) | |
| | 2-3 | QC_SMOKE_CONFIDENCE | Low | Medium | High |
| | 4-5 | QC_DUST_CONFIDENCE | Low | Medium | High |
| | 6 | SPARE | | | |
| | 7 | SPARE | | | |

*Start from the least significant bit

**Table 4 Product quality information flags for ABI aerosol detection product**

| Byte/Bit* | | Diagnostic Flag Name | Meaning | | |
|---|---|---|---|---|---|
| | | | 1bit: 0 (default) | 1 | |
| | | | 2bit: 00 (default) | 01 | 11 |
| 1 | 0 | QC_INPUT_LON | Invalid longitude | Valid longitude | |
| | 1 | QC_INPUT_LAT | Invalid latitude | Valid latitude | |
| | 2-3 | QC_INPUT_SOLZEN | Invalid solar zenith angle (SZA) 90<SZA or SZA <0 | Valid solar zenith angle(SZA) 0≤SZA≤90 | Solar zenith angle >60 |
| | 4-5 | QC_INPUT_SATZEN | invalid local zenith angle(VZA) 90<VZA or VZA <0 | Valid local zenith angle(VZA) 0≤VZA≤90 | Local zenith angle >60 |
| | 6-7 | QC_INPUT_SNOW/ICE_SOURCE | Snow/ice Mask from ABI retrieval | Snow/ice Mask from IMS | Snow/ice Mask from Internal test |
| 2 | 8 | QC_INPUT_SUNGLINT_SOURCE | ABI sun glint Mask | Internal sun glint Mask | |
| | 9 | QC_INPUT_SUNGLINT | outside of sun glint | within sun glint | |
| | 10 | QC_INPUT_LAND/WATER | Water | Land | |
| | 11 | QC_INPUT_DAY/NIGHT | Day | Night | |
| | 12 | QC_WATER_SMOKE_INPUT | Valid ABI inputs | invalid ABI inputs | |
| | 13 | QC_WATER_SMOKE_CLOUD | Cloud-free | Obscured by clouds | |
| | 14 | QC_WATER_SMOKE_SNOW/ICE | Snow/ice free | With snow/ice | |
| | 15 | QC_WATER_SMOKE_TYPE | Thin Smoke | Thick Smoke | |
| 3 | 16 | QC_WATER_DUST_INPUT | Valid ABI inputs | Invalid ABI inputs | |
| | 17 | QC_WATER_DUST_CLOUD | Cloud-free | Obscured by clouds | |
| | 18 | QC_WATER_DUST_SNOW/ICE | Snow/ice free | With snow/ice | |
| | 19 | QC_WATER_DUST_TYPE | Thin dust | Thick dust | |
| | 20 | QC_LAND_SMOKE_INPUT | Invalid ABI inputs | Valid ABI inputs | |
| | 21 | QC_LAND_SMOKE_CLOUD | Cloud-free | Obscured by clouds | |

| | | | | | |
|---|---|---|---|---|---|
| | 22 | QC_LAND_SMOKE_SNOW/ICE | Snow/ice free | With snow/ice | |
| | 23 | QC_LAND_SMOKE_TYPE | fire | Thick smoke | |
| 4 | 24 | QC_LAND_DUST_INPUT | Valid ABI inputs | Invalid ABI inputs | |
| | 25 | QC_LAND_DUST_CLOUD | Cloud-free | Obscured by clouds | |
| | 26 | QC_LAND_DUST_SNOW/ICE | Snow/ice free | With snow/ice | |
| | 27 | QC_LAND_DUST_TYPE | Thin dust | Thick dust | |
| | 28 | spare | | | |
| | 29 | spare | | | |
| | 30 | spare | | | |
| | 31 | spare | | | |

*Start from the least significant bit

**Table 5 Channel numbers and wavelengths for the ABI. Channels used in the ADP algorithm are highlighted in different colors. Key channels are identified by a check mark.**

| Future GOES Imager (ABI) Band | Nominal Wavelength Range (μm) | Nominal Central Wavelength (μm) | Nominal Central Wavenumber (cm-1) | Nominal sub-satelliteIGFOV (km) | Sample Use |
|---|---|---|---|---|---|
| 1 | 0.45-0.49 | 0.47 | 21277 | 1 | Dust/Smoke |
| 2 | 0.59-0.69 | 0.64 | 15625 | 0.5 | Dust/Smoke |
| 3 | 0.846-0.885 | 0.865 | 11561 | 1 | Dust/Smoke |
| 4 | 1.371-1.386 | 1.378 | 7257 | 2 | Dust/Smoke |
| 5 | 1.58-1.64 | 1.61 | 6211 | 1 | SMOKE |
| 6 | 2.225 - 2.275 | 2.25 | 4444 | 2 | Smoke |
| 7 | 3.80-4.00 | 3.90 | 2564 | 2 | Dust/Smoke |
| 8 | 5.77-6.6 | 6.19 | 1616 | 2 | |
| 9 | 6.75-7.15 | 6.95 | 1439 | 2 | |
| 10 | 7.24-7.44 | 7.34 | 1362 | 2 | |
| 11 | 8.3-8.7 | 8.5 | 1176 | 2 | |
| 12 | 9.42-9.8 | 9.61 | 1041 | 2 | |
| 13 | 10.1-10.6 | 10.35 | 966 | 2 | |
| 14 | 10.8-11.6 | 11.2 | 893 | 2 | Dust/Smoke |
| 15 | 11.8-12.8 | 12.3 | 813 | 2 | Dust/Smoke |
| 16 | 13.0-13.6 | 13.3 | 752 | 2 | |

Input for both Dust and smoke  Input for smoke  Input for dust

# 3 ALGORITHM DESCRIPTION

## 3.1 Algorithm Overview

The ADP serves to aid air quality forecasters in identifying smoke and dust laden atmosphere. The ADP algorithm follows heritage algorithms:

- Aerosols (dust) from AVHRR Extended (CLAVR-x) of NESDIS/STAR
- Non-cloud obstruction (including smoke and dust) detection in the MOD/MYD35 MODIS cloud mask developed for MODIS by the University of Wisconsin (UW).

The fundamental outputs of the ADP consist of four flags. They are the aerosol flag, smoke flag, dust flag and aerosol detection quality flags. Aerosol flag has a value of 0 for no aerosol and 1 for with aerosol. In the smoke/dust flag, 0 represents smoke/dust and 1 represents no smoke/dust, respectively. The details on quality flags are given in section 2.1. The following sections describe the ABI ADP algorithm.

## 3.2 Processing Outline

The processing outline of the ADP algorithm is summarized in Figure 1, which includes the basic modules as input, output, and detection over land and water. The algorithm is written in C++, and products are outputted in netCDF4 format. For optimizing CPU usage, the ADP algorithm is designed to run on segments of data. Each segment is comprised of multiple scan lines (10 lines).

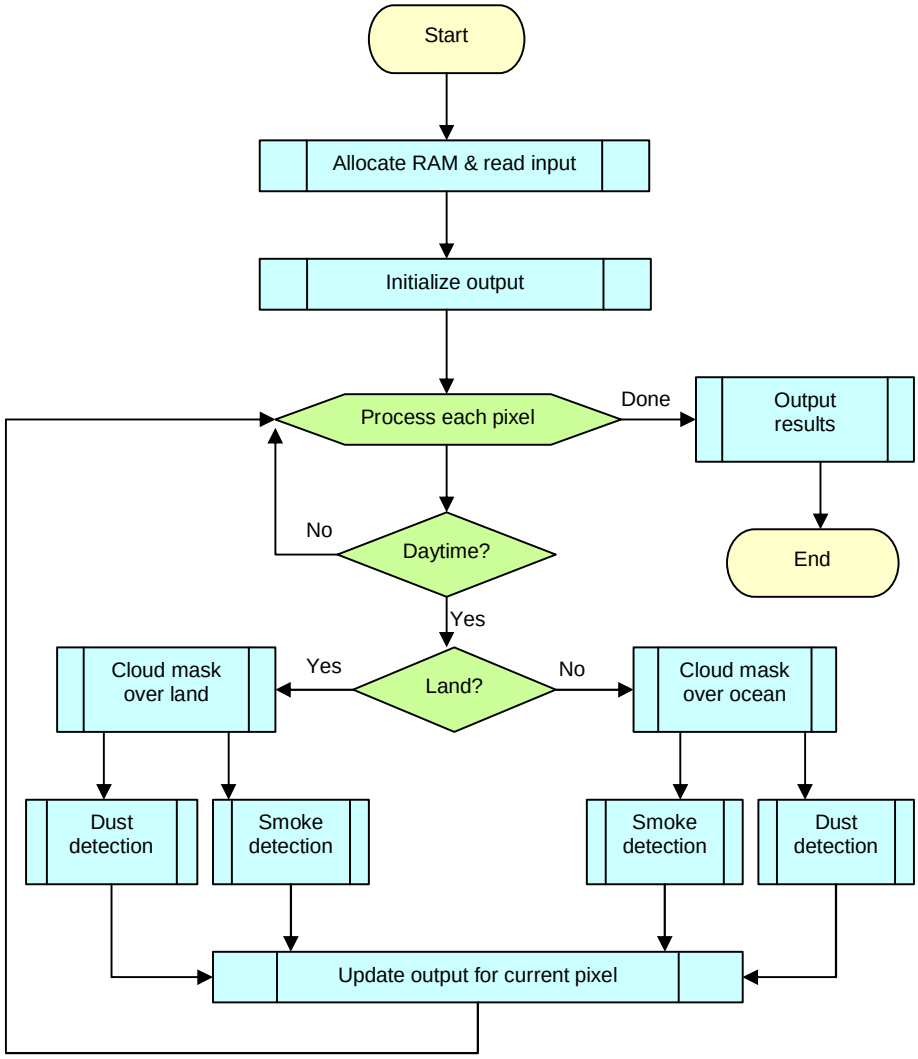


**Figure 1: High level flowchart of the ADP algorithm, illustrating the main processing sections.**

## 3.3 Algorithm Input

This section describes the input needed to process the ADP algorithm. While the ADP is derived for each pixel, it does require knowledge of the surrounding pixels. In its current operation, we run the ADP algorithm on segments of 10 scan-lines.

### 3.3.1 Primary Sensor Data

Calibrated/Navigated ABI reflectances and brightness temperatures on selected channels, geolocation (latitude/longitude) information, and ABI sensor quality flags are used as the sensor input data for the algorithm. **Error! Reference source not found.** contains the primary sensor data used by the ADP algorithm. The reflectance channel data with good quality will be averaged to the IR footprint resolution.

**Table 6 ADP primary sensor input data.**

| Name | Type | Description | Dimension |
|---|---|---|---|
| Ch1 reflectance | input | Calibrated ABI level 1b reflectance at channel 1 | grid (xsize, ysize) |
| Ch2 reflectance | input | Calibrated ABI level 1b reflectance at channel 2 | grid (xsize, ysize) |
| Ch3 reflectance | input | Calibrated ABI level 1b reflectance at channel 3 | grid (xsize, ysize) |
| Ch4 reflectance | input | Calibrated ABI level 1b reflectance at channel 4 | grid (xsize, ysize) |
| Ch6 reflectance | input | Calibrated ABI level 1b reflectance at channel 6 | grid (xsize, ysize) |
| Ch7 brightness temperature | input | Calibrated ABI level 1b brightness temperature at channel 7 | grid (xsize, ysize) |
| Ch 14 brightness temperature | input | Calibrated ABI level 1b brightness temperature at channel 14 | grid (xsize, ysize) |
| Ch 15 brightness temperature | input | Calibrated ABI level 1b brightness temperature at channel 15 | grid (xsize, ysize) |
| Latitude | input | Pixel latitude | grid (xsize, ysize) |
| Longitude | input | Pixel longitude | grid (xsize, ysize) |
| QC flags | input | ABI quality control flags with level 1b data | grid (xsize, ysize) |

Note that, the cloud mask required in ADP algorithm is designed to primarily come from ABI cloud product. Channels used to determine the cloud mask are not listed here as that information is part of the cloud mask ATBD.

### 3.3.2 ABI Product Precedence and Ancillary Data

The dynamic data are from both ABI Level-1b and Level-2 products needed by the ADP algorithm are listed in Table 7. They include cloud mask from ABI cloud product, snow/ice mask from ABI level-2 product, sun glint mask and day/night flag are determined internally in the ADP algorithm from viewing and illuminating geometry information.

**Table 7 ABI Product Precedence and Ancillary input data.**

| | Name | Type | Source | Dimension |
|---|---|---|---|---|
| ABI Product Precedence Data | Cloud mask | input | ABI level 2 cloud product | grid (xsize, ysize) |
| | Snow/Ice mask | input | ABI level 2 Snow/Ice Product | grid(xsize, ysize) |
| | Sun glint mask | input | Internally determined but needs information on viewing geometry | grid(xsize, ysize) |
| | Day/night flag | input | Internally determined but needs information on viewing geometry | grid(xsize, ysize) |
| Ancillary Data | Land/Water mask | Input | 1 km dataset http://glcf.umiacs.umd.edu/data/landcover | grid(xsize,ysize) |

- **Snow/Ice mask**

Primary source of snow/ice is ABI Level-2 Snow/Ice Product. However, under the situation that the primary source is missing, Interactive Multisensor Snow and Ice Mapping System (IMS) (http://nsidc.org/data/g02156.html) snow/ice mask will be the secondary source. In addition, the ADP algorithm has internal snow/ice test over land,

whose function is to eliminate the residuals from external snow/ice mask over land. It is applied after the primary /secondary snow/ice mask. Details on the internal snow/ice mask are given in section 3.4.2.1.

- **Cloud mask**

The purpose of using cloud mask in the ADP algorithm is to eliminate pixels with obvious clouds, such as high and ice cloud, before performing smoke/dust detection. Hence, the requirement of ADP algorithm for cloud mask is more specific than just cloud or clear mask. Stringent cloud mask has the potential to classify smoke as cloud, while loose cloud mask increases the chance of misidentifying clouds as smoke. The ADP algorithm intends to use only individual tests in ABI cloud mask product which indicate the existence of high cloud, ice cloud and thin cirrus cloud. However, this dependency was not tested because ABI cloud algorithm was not ready to run on MODIS. Efforts will be put once common proxy data become available. Currently, the ADP algorithm is using MODIS data as proxy, including MODIS cloud mask. Based on the definition of individual test from both ABI cloud mask and MODIS cloud mask, the individual test used in ADP algorithm is mapped to ABI cloud mask and they are given in **Error! Reference source not found.**.

**Table 8 Mapping of ABI ADP cloud mask tests to ABI cloud mask tests**

| MODIS cloud mask tests used by ABI ADP Bit No. | ABI Cloud mask tests Byte No. (Bit No.) | Description | Locations where the tests are used in ADP |
|---|---|---|---|
| 9 | 3 (7) | CIRREF- Near IR Cirrus Test (1.38 μm) | Smoke over land<br>Smoke over water<br>Dust over land<br>Dust over Water |
| 15 | 2 (4)<br>+<br>3 (3) | ETROP – Emissivity at Tropopause Test<br>+<br>ULST – Uniform Low Stratus Test<br>when ETROP is true but ULST is false | Smoke over Water<br>Dust over water<br>Smoke over land<br>Dust over land |
| 16 | 3( 7 ) | CIRREF- Near IR Cirrus Test (1.38 μm) | Smoke over Water<br>Smoke over Land |
| 18 | 2 (5) | PFMFT – Positive FMFT (Split-Window BTD) Test | Smoke over water<br>Dust over water<br>Smoke over land<br>Dust over land |
| 19 | 3 (2) | EMISS4 – 4 μm Emissivity Test | Smoke over land |
| 20 | 3 (4) | RGCT – Reflectance Gross Contrast Test | Smoke over land |

- **Sun glint mask**

The ADP algorithm is designed to generate internal sun glint mask based on ABI viewing and illuminating angles as second source. The sun glint angle (η) is calculated as follows

$$\cos(\eta) = \cos(\theta_0) * \cos(\theta) + \sin(\theta_0) * \sin(\theta) * \cos(180 - \varphi)$$

$\theta_0$ : *solar zenith angle*

$\theta$ : *satellite zenith angle*

$\varphi$ : *relative azimuth angle*

Note that, φ is defined as the difference between satellite azimuth angle and solar azimuth angle. An area with calculated sun glint angle greater than zero and less than $40^o$ is defined as sun glint area.

- **Day/night mask**

A day/night flag is determined internally based upon the solar zenith angle. Day is defined as solar zenith angle of less than $87^o$, while night is defined as solar zenith angle greater than $87^o$.

- **Land/water mask**

The only static input data required by the ADP algorithm is a global 1km land/water mask. The global land cover classification collection created by The University of Maryland Department of Geography with Imageries from the AVHRR satellites acquired between 1981 and 1994 [Hansen et al., 1998] is the source (http://glcf.umiacs.umd.edu/data/landcover/).

## 3.4 Theoretical Description

The ADP algorithm attempts to separate cloudy and clear pixels from those with smoke or dust. The detection of smoke or dust relies on the distinctive signature of smoke or dust which is often expressed in terms of spectral variations of the observed brightness temperature or solar reflected energy. The spectral variation of the refractive index plays an important role in the success of these methods. In addition, the scattering and absorption properties of an aerosol also depend on the particle size distribution and the particle shape. Several aerosol remote sensing techniques have been developed using observations from the Advanced Very High Resolution Radiometer (AVHRR) [e.g. Barton et al., 1992]. Similar to the dust plumes, the volcanic ash plumes often generate negative brightness temperature differences between 11μm ($BT_{11}$) and 12 μm ($BT_{12}$). Prata [1989] has demonstrated the detection of volcanic aerosols using two infrared channels, while Ackerman and Strabala [1994] applied observations at 8.6, 11 and 12μm from the Hyper Spectral Infrared Sound (HIRS) instrument to study the Mt. Pinatubo stratospheric aerosol.

Image based aerosol detection always involves assumptions of the radiometric characteristics of aerosol, clear and cloudy scenes. The surface conditions also influence the separation of aerosol pixels from those with clear-sky or cloud. The ADP algorithm currently uses spectral and spatial tests to identify pixels with smoke or dust in the daytime. Temporal tests are planned for future versions of the algorithm. The algorithm also treats the detection differently for water and land.

### 3.4.1 Physics of the Problem

Techniques for the remote sensing of aerosols using solar and thermal measurements from satellites have been developed for several instruments, including AVHRR and MODIS. Fundamentally, these methods are based on the radiative signatures of

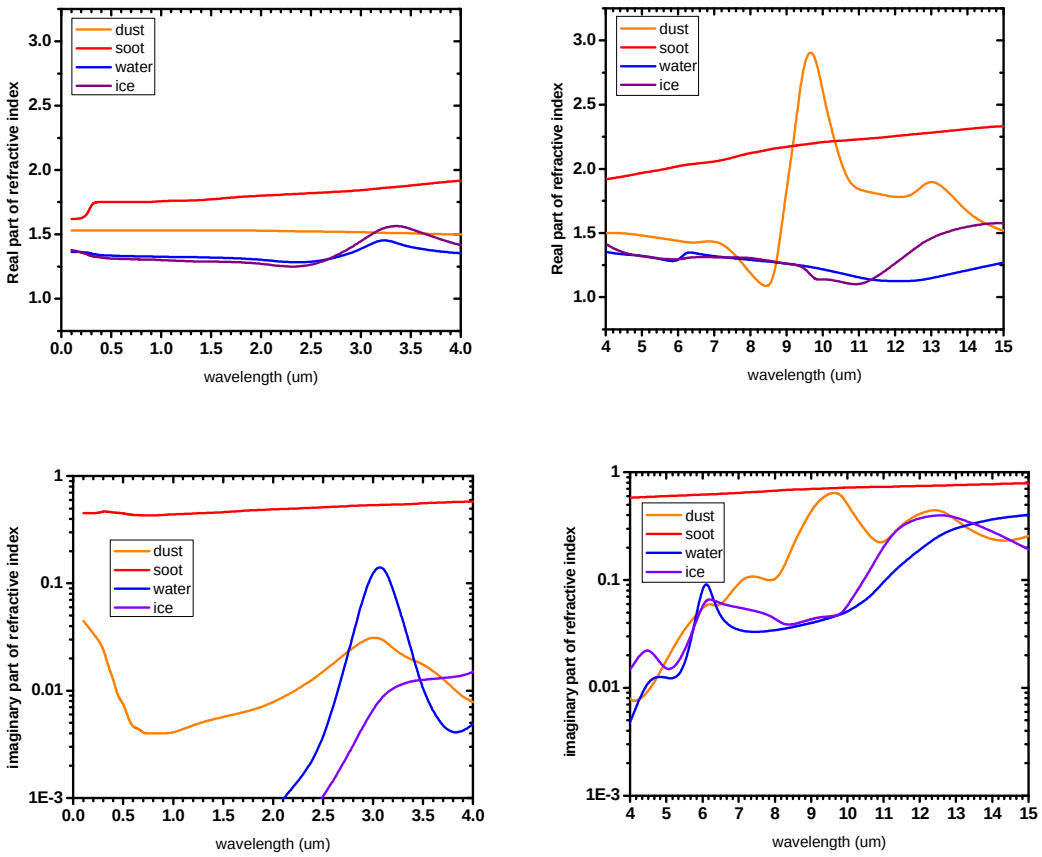


**Figure 2: Real and imaginary part of dust, soot, water and ice as a function of wavelength. Plots are based on data obtained from CRTM.**

aerosols. The problem of accurate detection and classification is compounded by the fact that the physical characteristics of aerosols (e.g. particle size distribution, concentration, chemical composition, location in the atmosphere) change as the aerosol layer develops and dissipates. These physical changes are capable of affecting the radiative characteristics of the original aerosol and our capability to detect them from satellite observations. In addition to being present at the source region, aerosols are transported by winds to other regions of the globe.

Fundamentally, the radiative signatures of an aerosol layer are determined by the scattering and absorption properties of the aerosol within a layer in the atmosphere. These are:

- Extinction coefficient, $\sigma_{ext}$ (which integrated over path length gives the optical thickness, $\tau$). This parameter characterizes the attenuation of radiation through an aerosol volume due to aerosol scattering (measured by scattering coefficient $\sigma_{sca}$) and absorption (measured by absorption coefficient $\sigma_{abs}$) so that $\sigma_{ext}$= $\sigma_{sca}$+ $\sigma_{abs}$.
- Single scattering albedo, $\omega_{\circ} = \sigma_{sca} / \sigma_{ext}$ , which describes how much attenuation of radiation is due to scattering. It ranges between 1 for a non-absorbing medium and 0 for a medium that absorbs and does not scatter energy.
- Phase function, $P(\mu, \mu')$ which describes the direction of the scattered energy. Here $\mu$ and $\mu'$ are the cosine of solar and local zenith angles, respectively.

There are three important physical properties of a particle that are needed to determine the scattering and absorption properties listed above:

- The index of refraction ( $m = m_r - im_i$ ) of the particle: The index of refraction of the medium is also required, but for air it is 1. Measurements of the index of refraction of a material are very difficult to make [Bohren and Huffman 1983]. The $m_r$ is an indication of the scattering properties while the $m_i$ is an indication of the absorption characteristics of the material. The scattering and absorption properties of an aerosol also depend on the particle size distribution. The index of refraction of smoke and dust is different from ice or water (Figure *2*), which suggests that multi-spectral techniques should be useful in separating the aerosol from clouds.
- The shape of the particle: Microscopic analysis reveals that aerosols are irregular in shape. Thus, the assumption of spherical particles is often not accurate but a reasonable approximation. Shape effects may be a particular problem in the vicinity of strong infrared absorption bands for small particles with a uniform size distribution [Bohren and Huffman, 1983]. As no satisfactory method of handling the radiative properties of irregular shaped particles has been developed for general application to remote sensing techniques, the sensitivity studies generally assume spherical shaped particles.
- The size distribution of the particles, n(r): In addition to defining the radiative properties, the n(r) also determines the aerosol mass concentration. Particle size distributions of aerosols are often expressed as a log-normal distribution.

Because of these distinctive wavelength dependent aerosol properties, the spectral threshold based techniques are used to detect dust, smoke, volcanic ash work. The bulk transmittance of many aerosols displays a strong spectral variation in the 8-10 μm and 10-12 μm regions. This is also a spectral region over which the atmosphere is fairly transparent. For these reasons, techniques have been developed which successfully employ satellite radiance measurements at 11 and 12 μm to detect aerosols. These split window IR techniques have primarily been applied to volcanic aerosols, particularly those from sulfur-rich eruptions [e.g. Prata 1989; Barton et al. 1992] as well as dust outbreaks [Legrand et al., 1992, 2001; Evan et al., 2006]. As demonstrated in Figure 3,

dust absorbs more radiation at 12µm than 11µm, which causes the brightness temperature difference between the two to be negative.

There is absorption and emission of water vapor in the 11 and 12 µm channels. Because the weighting function for the 11µm channel peaks lower in the atmosphere than the 12µm channel does, the presence of a dry air mass, often associated with dust events, will tend to reduce the positive $BT_{11\mu m}$-$BT_{12\mu m}$ values associated with clear sky atmospheres. In addition, dust has a larger absorption at 12µm than at 11µm, so that dust plumes generally have a higher emissivity and lower transmissivity in the 12 µm channel [Ackerman, 1997; Dunion and Velden, 2004]. For more elevated dust layers, the increased temperature separation between the dust layer and the surface, and coincident reduction of dry air closer to the peak of the 11µm weighting function makes the split window brightness temperature difference less positive. This difference has also been observed to be affected by the optical thickness of a given dust plume, so that in thick optical depths the $BT_{11\mu m}$-$BT_{12\mu m}$ difference becomes more negative.

Darmenov and Sokolik [2005] further explored the brightness temperature difference technique using MODIS data applied to dust outbreaks from different regions of the globe. In general, $BT_{8\mu m}$-$BT_{11\mu m}$ becomes less negative and $BT_{11\mu m}$-$BT_{12\mu m}$ becomes more negative with increasing dust loading (Figure ***3***). However, in the ADP algorithm, the 3.9 µm is chosen instead of 8 µm because 3.9 µmhas lees water vapor absorption and also to eliminate the false alarm from low level clouds (often towering cumulus).

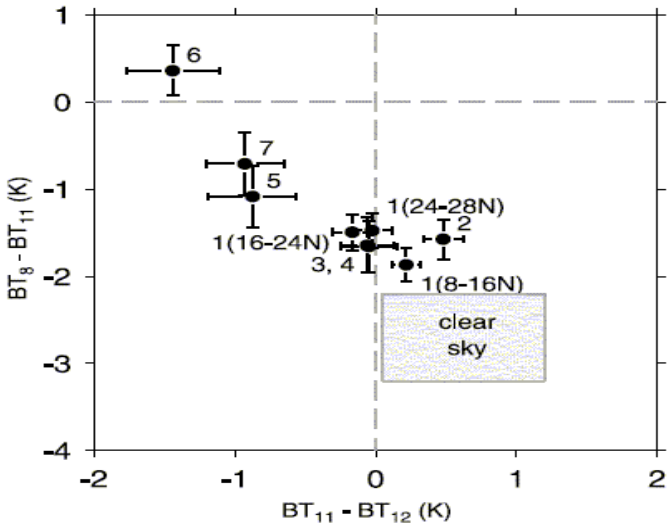


**Figure 3. Combined tri-spectral diagram of brightness temperature differences for ‘‘heavy dust’’ pixels. From Darmenov and Sokolik [2005].**

Dust absorbs at blue wavelengths and appears visually brown in color. Clouds are spectrally neutral and appear white to human eyes. For this reason, the reflectances at 0.86, 0.47 and 0.64µm have been used to identify dust. This is often done in a ratio of one to another or as a normalized difference index. For example, the MODIS aerosol optical depth retrieval algorithm has a condition that ratio of reflectances between 0.47 µm and 0.64 µm should be less than 0.75 for the central pixel in a 3 X 3 box to be identified as

dust. Evan et al [2006] use a constraint that the reflectance value of the 0.86µm channel ($R_{0.86\mu m}$) divided by the reflectance value of the 0.63µm channel ($R_{0.63\mu m}$) is within the range of 0.6–1.0 for the AVHRR (this range is slightly different for MODIS due to differences in the spectral response functions). Again, due to the nonlinear relationship with optical thickness, we chose to square the reflectances prior to applying a test. The physical basis for this test is that the presence of smaller aerosols, like smoke, tends to reduce the values for this ratio, as smaller particles are more efficient at scattering light at 0.63µm. Although dust particles are observed to scatter more light at 0.63µm than at 0.86 µm probably due to their size, they tend to exhibit more uniform scattering across this spectral region [Dubovik et al., 2002]. A ratio type test of $R_{0.86\mu m}$/ $R_{0.63\mu m}$ has been found to be useful in discriminating pixels containing smoke from those with dust

Although dust particles are observed to scatter more light at 0.63µm than at 0.86µm probably due to their size, they tend to exhibit more uniform scattering across this spectral region [Dubovik et al., 2002]. Thus, the ratio $R_{0.86\mu m}$/ $R_{0.63\mu m}$ test [Evan et al., 2006] has been found to be useful in discriminating pixels containing smoke from those with dust. Another test for dust examination over water is the requirement that the ratio of reflectance at 0.47 µm and 0.64 µm is smaller than 1.2. Similar to the dust detection over land, low level clouds (often towering cumulus) can also have a negative split window brightness temperature difference. Therefore, brightness temperature between 3.9 µm and 11 µm can be used to screen out cloud contaminated pixels.

The RGB image in Figure ***4*** shows a dust plume with different regions of heavy dust, thin dust, and clear sky clearly identified. For these different regions, the relationship between different visible and IR BTD are plotted in the four panels of Figure *4*. Clear sky pixels have low reflectance at both 0.47 and 0.64 um, thin dust has elevated reflectances at these channels, and thick dust pixels have 20% or greater reflectance at these channels. The BTD between 3.9 um and 11 um plotted against the BTD between 11 µm and 12 µm shows a clear separation of thick dust pixels compared to thin dust and clear-sky.

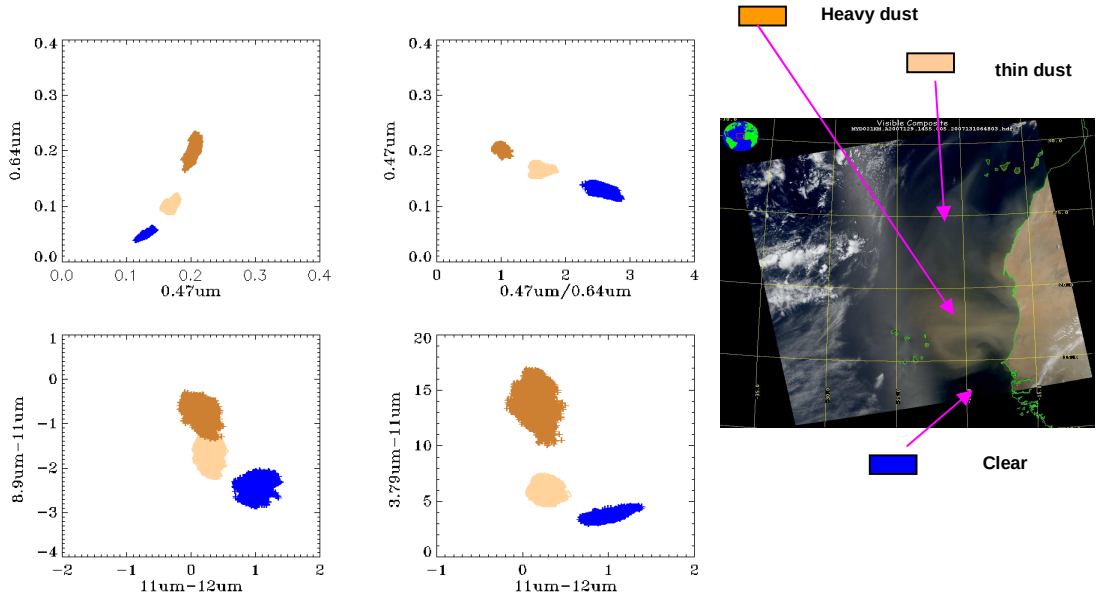


**Figure 4: The relationship between various combinations of channels for heavy, thin dust, and clear conditions.**

For smoke tests, fire spots are detected by looking at pixels with BTs at 3.9 µm greater than 350K and the BTD between 3.9 µm and 11 µm greater than or equal to 10K. Pixels that pass fire test are assumed to have smoke. The smoke tests over land take advantage of a linear relationship observed between MODIS reflectance at 0.63 µm and 2.13 µm (Figure ***5***). This relationship gets noisy when reflectance at 2.13 µm is greater than 20%. When smoke is present in a pixel, there is a larger increase in $R_{0.64\mu m}$ than $R_{2.25\mu m}$.

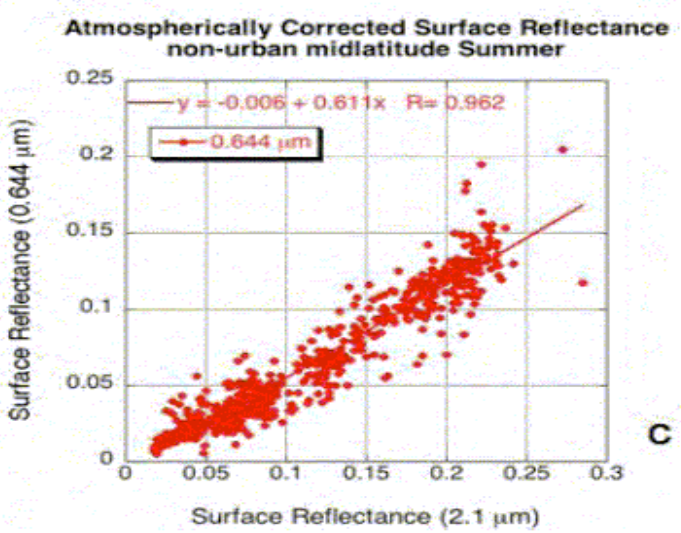


**Figure 5 : Surface reflectance at 0.64µm va. surface reflectance at 2.1µm from MODIS. (Reference: Remer et al. 2005)**

Smoke is separated from cloud using spatial uniformity tests for 0.64 µm channel. Clouds show large variability in this channel compared to smoke.

Spatial variability tests will also help in avoiding the mis-classification of clouds as smoke. By using the standard deviation of reflectance at 0.86um, where both smoke aerosols, thick clouds show uniform variability compared to thin smoke and partially cloudy pixels. Also, while reflectance from cloud is spectrally independent, it is not for smoke. This allows the use of spectral contrast tests using 0.47 um, 1.61 um, and 2.25 µm to separate clouds from thick smoke. A combination of tests developed using multiple channels are shown in Figure 6.

First of all, over water, clear pixels, pixels loaded with thick smoke and cloud are more uniform than pixels with partial cloud or thin dust. By using the standard deviation of reflectance at 0.86um, where both aerosol and clouds effects are moderate, pixels which contain thick smoke vs. clouds/thin smoke can be separated. It is known that smoke in visible channels looks brighter than water surface but darker than a cloud. However, it is very difficult to completely separate them by only using the reflectance test. Therefore, based on the fact that reflection from clouds is spectrally independent, while reflection from smoke has strong wavelength dependence, spectral contrast tests are combined to separate clouds, smoke and water surface. First of all, the ratio between 0.47µm to 1.61µm is used, the rationale for choosing these two channels is due to the fact that aerosol effect is larger at 0.47um but water is darker at 1.61um. Secondly, the ratio between 2.25µm to 1.61µm is combined to enhance the separation of smoke from clouds. Thirdly, by constraining R0.47µm and R1.61µm, thick smoke can be identified

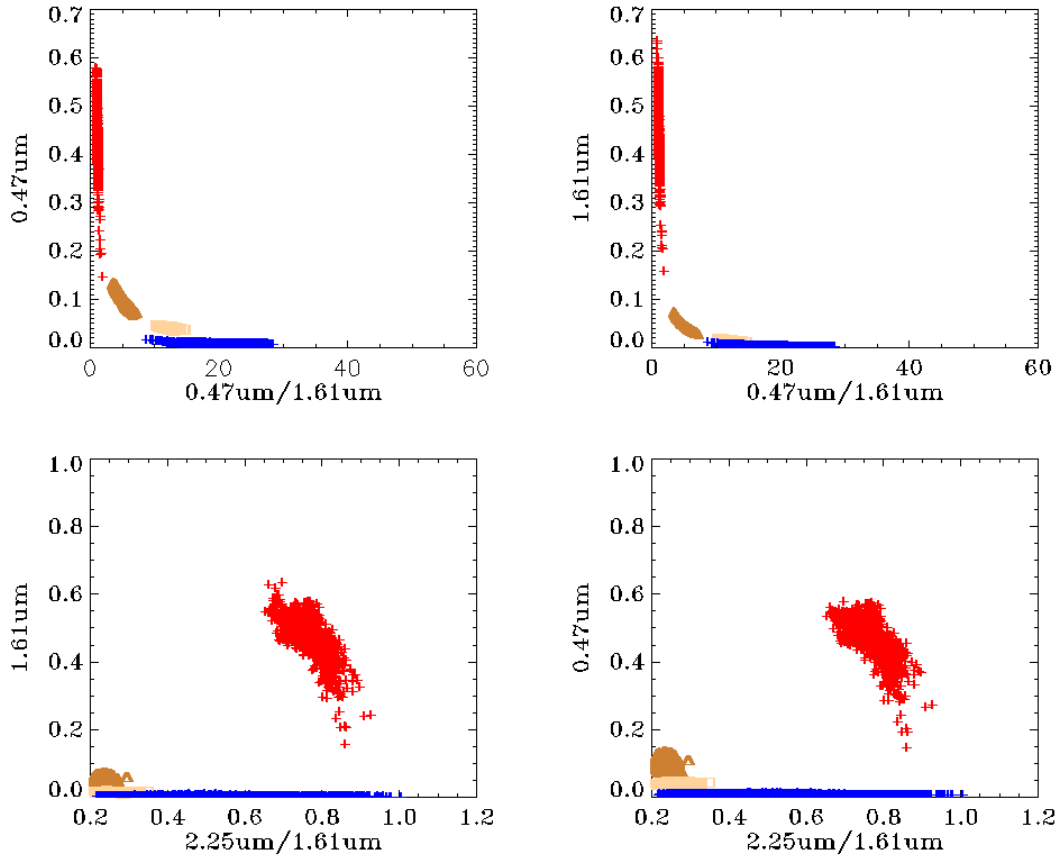


**Figure 6: Scatter plots of $R_3$ vs. $R_{0.47\mu m}$, $R_3$ vs. $R_{1.61\mu m}$, $R_4$ vs. $R_{0.47\mu m}$, $R_4$ vs. $R_{1.61\mu m}$ for clear-sky pixels (blue), thick smoke pixels (dark brown), thin smoke (light brown) and cloudy pixels (red). Definitions of $R_3$ and $R_4$ are given in section 3.4.2.**

### 3.4.2 Mathematical Description

Computation of binary flag for smoke/dust in the ADP algorithm is a process of elimination and determination. It has three levels. First, any pixel which contains cloud (high and optically thick clouds) and snow/ice, determined from input cloud mask and snow/ice mask, is tagged as a cloudy pixel and not processed. Second, pixels contaminated by clouds but not screened by cloud mask are further identified by a combination of spectral and spatial variability tests. Third, spectral variability tests determine if a pixel has smoke or dust. Due to the fact that the contrast of smoke/dust to underlying surface is different for land and water, computation of binary flag for smoke/dust in the ADP is separated for land and water. The following sections describe the various tests employed in the ADP algorithm. The symbols and formulae used in the various tests through the ADP algorithm are defined as follows:

$$Rat_1 = \frac{R_{0.64\ \mu m} - R_{0.47\ \mu m}}{R_{0.64\ \mu m} + R_{0.47\ \mu m}}$$

$$Rat_2 = \frac{Rat_1^2}{R_{0.47\ \mu m}^2}$$

$$NDVI = \frac{R_{0.86\ \mu m} - R_{0.64\ \mu m}}{R_{0.86\ \mu m} + R_{0.64\ \mu m}}$$

In the formulae listed above, “Rat” is for ratio, “NDVI” is Normalized Difference Vegetation Index, “MNDVI” is Modified Normalized Difference Vegetation Index, “R” is reflectance. Additionally variables such as “BT” for Brightness Temperature, “BTD” for Brightness Temperature Difference, “StdR” for Standard Deviation of Reflectence computed spatially for 3 X 3 pixels.

Calculation of StdR for pixel which is not on the edge of scan is from the surrounding 3 by 3 pixels. For pixels on the edge of scan, standard deviation for the closest pixel is assigned.

### 3.4.2.1 Snow/ice test over land

Before proceeding to any tests over land, it is important to identify pixels contaminated by snow/ice As described earlier, ABI snow/ice product is the primary source, and snow/ice mask from IMS is used as a second source. However, a further test is designed to catch any pixels that pass through but have snow/ice.
The specific tests as currently implemented are:

1) Good data test
   - $R_{0.86\mu m}$, $R_{1.61\mu m} > 0$ &
   - $BT_{11\mu m} > 0K$ &
   - ABI quality flags for above channels indicate good data

2) Snow and Ice tests;
   if $BT_{11\mu m} \leq 285k$ & $(R_{0.86\mu m} - R_{1.61\mu m}) / (R_{0.86\mu m} + R_{1.61\mu m}) > 0.01$
   then snow/ice indicated for all pixels within 5 X 5 $km^2$.

The results from utilizing these internal snow/ice tests show that false snow detections from the original MODIS product are removed.

### 3.4.2.2 Dust Detection over Land

Figure 7 is a flow chart of the algorithm to detect the presence of dust over land during daytime (defined as solar zenith angle less than $87^o$ degrees). The tests are not performed over snow and ice or in the presence of clouds.

The specific tests as currently implemented are:

(1) Test for the presence of snow/ice by first using ABI mask and then using internal snow/ice test. Also test for the presence of clouds by using ABI cloud mask. Any pixel with positive snow/ice/cloud mask is not processed.

(2) Test for the quality of the input radiance data

- $R_{0.47\mu m}$, $R_{0.64\mu m}$, $R_{0.86\mu m}$, $R_{1.38\mu m} > 0$ &
- $BT_{3.9\mu m}$, $BT_{11\mu m}$, $BT_{12\mu m} > 0K$ &
- ABI quality flags for above channels equal to zero, indicating quality of the data is assured.

(3) Thin Dust detection: BTD and R tests – check for pixels with thin dust and no cirrus clouds

If
$BT_{11\mu m}$-$BT_{12\mu m} \leq$ -0.2K & $BT_{3.9\mu m}$- $BT_{11\mu m} \geq$ 15K & $R_{1.38\mu m} < 0.035$
then begin
If
MNDVI < 0.08 & $Rat_2 > 0.005$
then thin dust
else
If
$BT_{3.9\mu m}$- $BT_{11\mu m} \geq$ 20K then thin dust
endelse
endif
endif

(4) Thick dust test

If
$BT_{11\mu m}$-$BT_{12\mu m} \leq$ -0.5K & $BT_{3.9\mu m}$- $BT_{11\mu m} \geq$ 25K & $R_{1.38\mu m} < 0.055$
and
MNDVI < 0.2 then dust

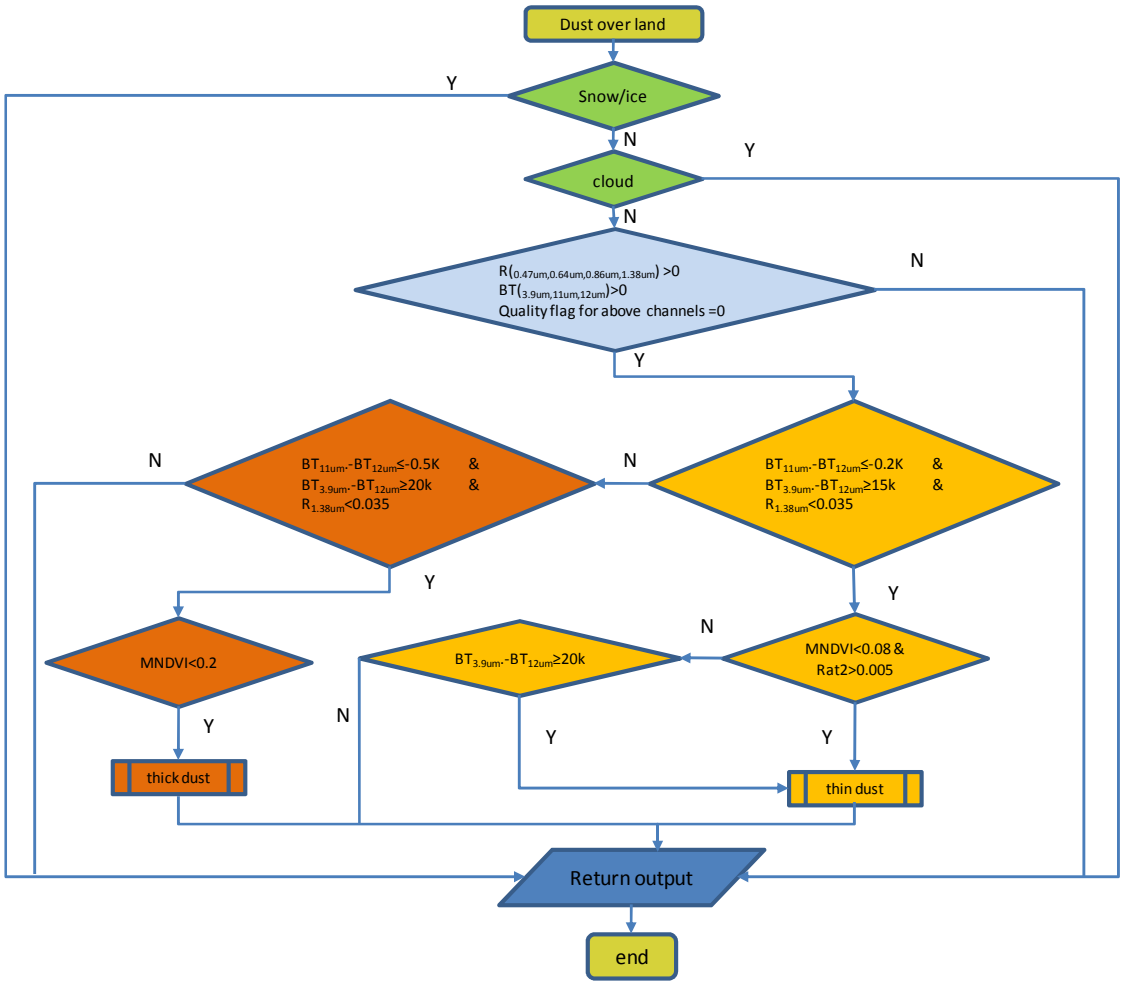


**Figure 7: Detail Flow chart of dust detection over land.**

### 3.4.2.2.1 Example result

The results of an application of the dust test to MODIS Aqua data on April 15, 2003 at 20:20 UTC is shown in Figure 8. The left hand side of the figure is a red-green-blue (RGB) false color image of the scene showing the location of the dust outbreak. The right-hand side of the figure shows the results of the dust test. Pixels flagged as dusty are colored orange. A second example is shown in Figure 9.

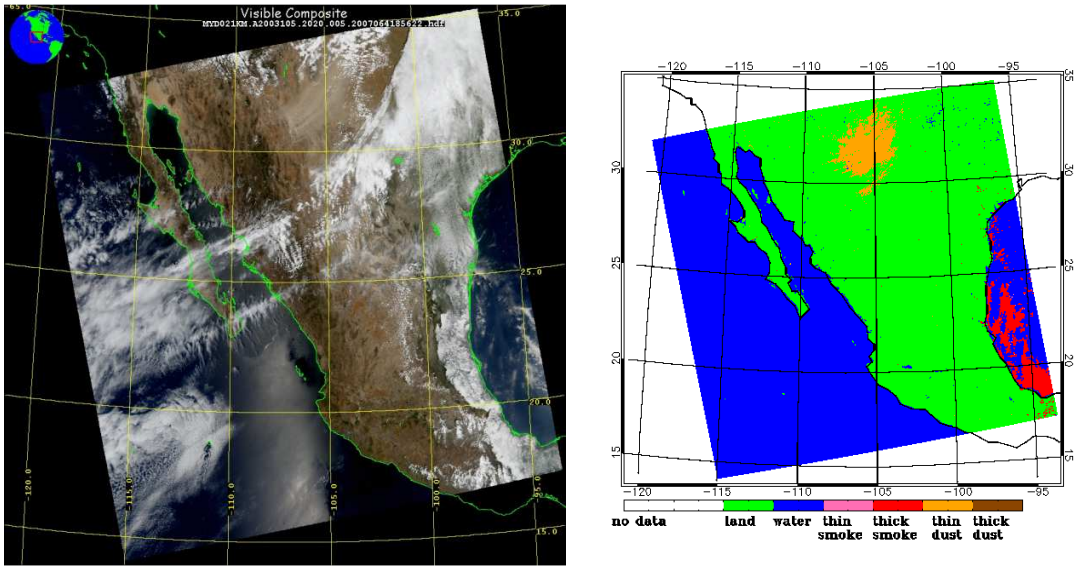


**Figure 8: Left: a red-green-blue (RGB) false color image of a MODIS Aqua observation data on April 15, 2003 at approximate 20:20 UTC. Right: the results of the dust test where pixels flagged as dusty are colored orange.**

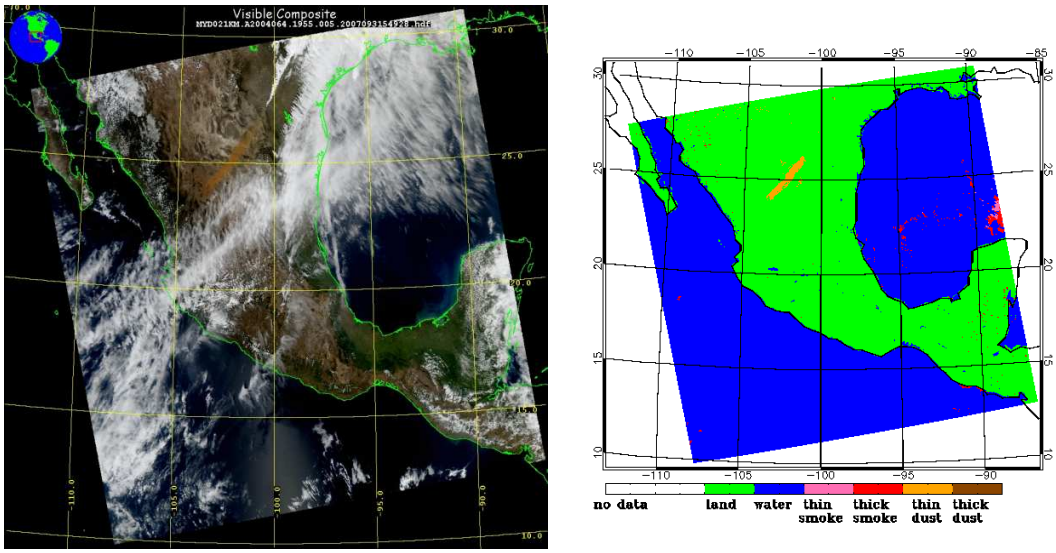


**Figure 9: Left: a red-green-blue (RGB) false color image of a MODIS Aqua observation data on March 4, 2004 at approximate 19:55 UTC. Right: the results of the dust test where pixels flagged as dusty are colored blue.**

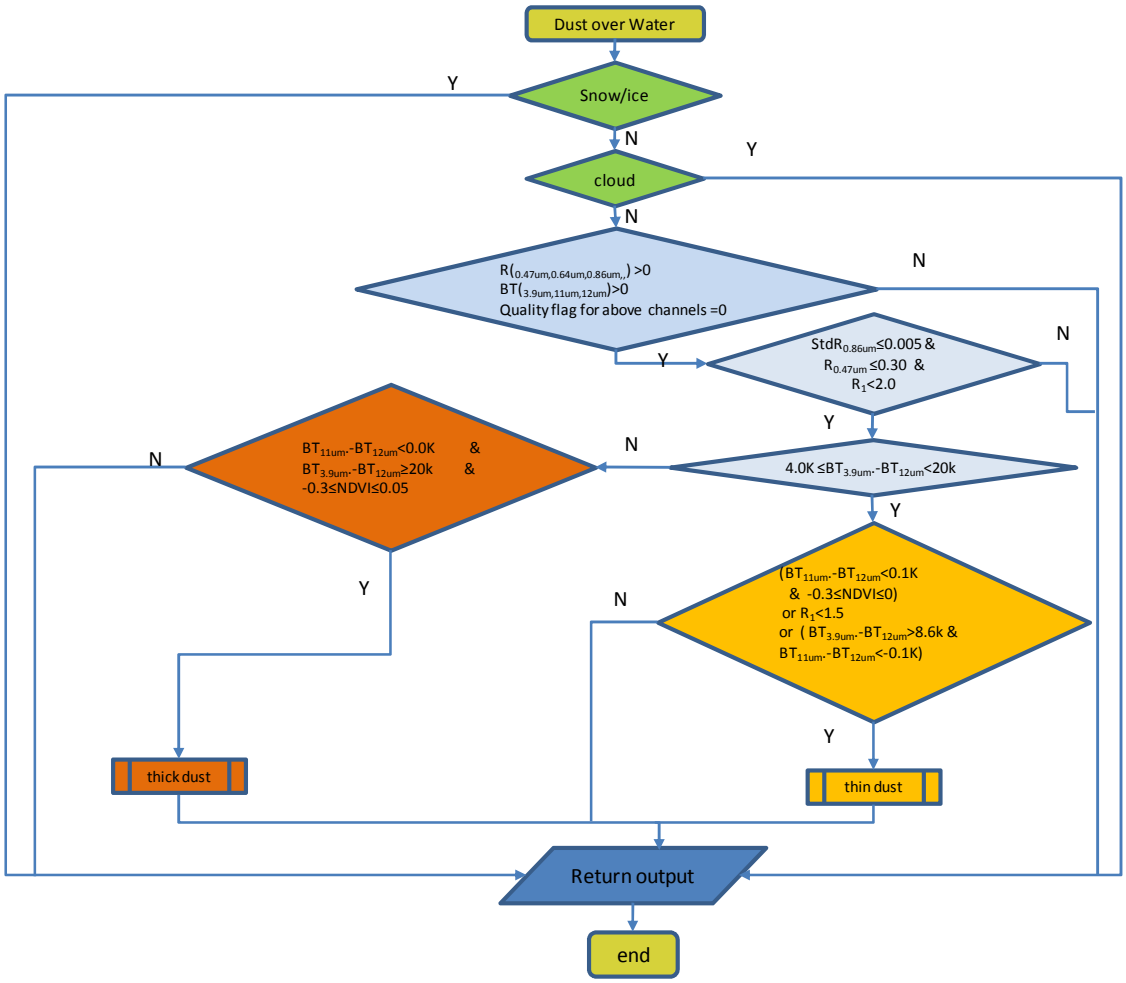


**Figure 10: Detailed flow chart of dust detection over water.**

### 3.4.2.3 Dust Detection over Water

Figure 10 is a detailed flow chart of the algorithm to detect the presence of dust over water during the daytime. The tests are not performed over snow and ice or in the presence of ice clouds.

The specific tests as currently implemented are

1) Test for the presence of snow/ice by first using primary /secondary snow/ice mask. Also test for the presence of clouds by using ABI cloud mask. Pixel is considered to be obscured by clouds if any of ABI cloud mask tests in 3/7 (byte no./bit no.), 2/5 and 2(4) +3(3) is true. Any pixel with positive snow/ice/cloud mask is not processed.

2) Test for the quality of the input radiance data

   - $R_{0.47\mu m}$, $R_{0.64\mu m}$, $R_{0.86\mu m} > 0$ &
   - $BT_{3.9\mu m}$, $BT_{11\mu m}$, $BT_{12\mu m} > 0K$

- ABI quality flags for above channels equal to zero, indicating quality of the data is assured.

3) Uniformity and spectral tests for residual clouds

- $MeanR_{0.86\mu m} > 0$ and $StdR_{0.86\mu m} \leq 0.005$ &
- $R_{0.47\mu m} \leq 0.3$ &
- $R_1 < 2.0$

4) Tests for dust

If $4K < BT_{3.9\mu m} - BT_{11\mu m} \leq 20K$ then thin dust test
Else
Thick dust test

4.1 thin dust test

if
$BT_{11\mu m} - BT_{12\mu m} < 0.1K$ and $-0.3 \leq NDVI \leq 0$ and
$R_{0.47\mu m}/R_{0.64\mu m} < 1.7$ and
$BT_{3.9\mu m} - BT_{11\mu m} > 10K$ and $BT_{11\mu m} - BT_{12\mu m} < -0.1K$
then thin dust

4.2 thick dust test

if
$BT_{3.9\mu m} - BT_{11\mu m} > 20K$ and
$BT_{11\mu m} - BT_{12\mu m} \leq 0K$ and $-0.3 \leq NDVI \leq 0.05$
then thick dust

5) Set dust mask flag

There are three separate tests for dust over water, each is elaborated below. Any of the tests can pass for the pixel to be flagged as dusty, although some of the tests have multiple conditions that must be passed.

### 3.4.2.3.1 Example result

The results of an application of the dust test to MODIS data on May 18, 2010 at approximate 12:30 UTC is shown in Figure 11. The left hand side of the figure is a RGB images, the middle image is MOIDIS AOD (large than 0.2) the brightness. The image to the right shows the results of the water and land dust detection algorithm, where orange and brown regions indicate the presence of dust.

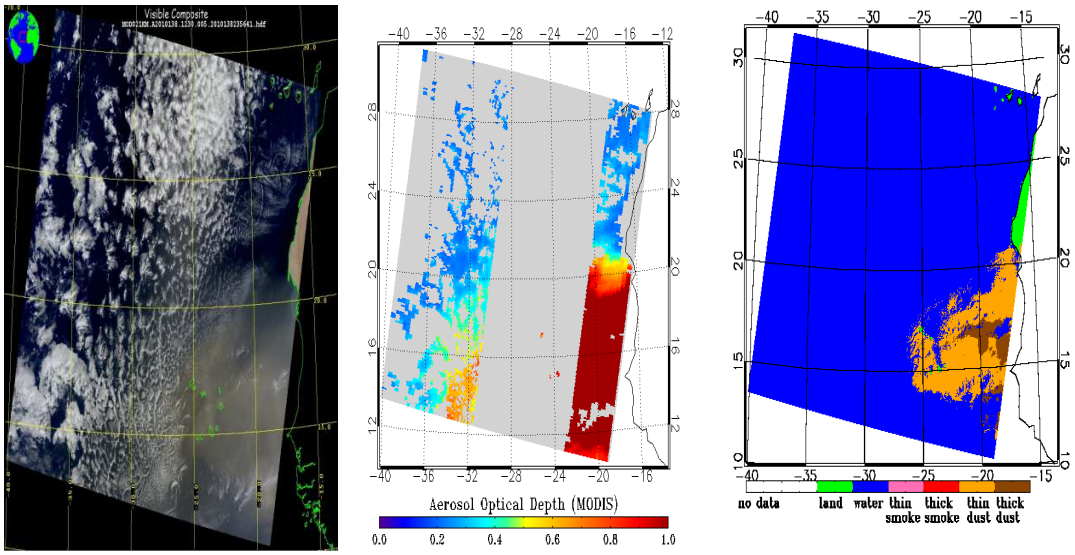


**Figure 11: MODIS Terra observations on May 18, 2010 at approximate 12:30 UTC. A dust outbreak is flowing from the Sahara desert over the adjacent Atlantic Ocean.**

The MODIS AOD image shows no data over sun glint region. The RGB image and the ABI dust mask image show qualitative agreement.

### 3.4.2.4 Thick Smoke Detection over Land

Figure 12 is a detailed flow chart of the algorithm to detect the presence of smoke over land during daytime. Note that, the tests are not performed in the presence of snow/ice and ice clouds

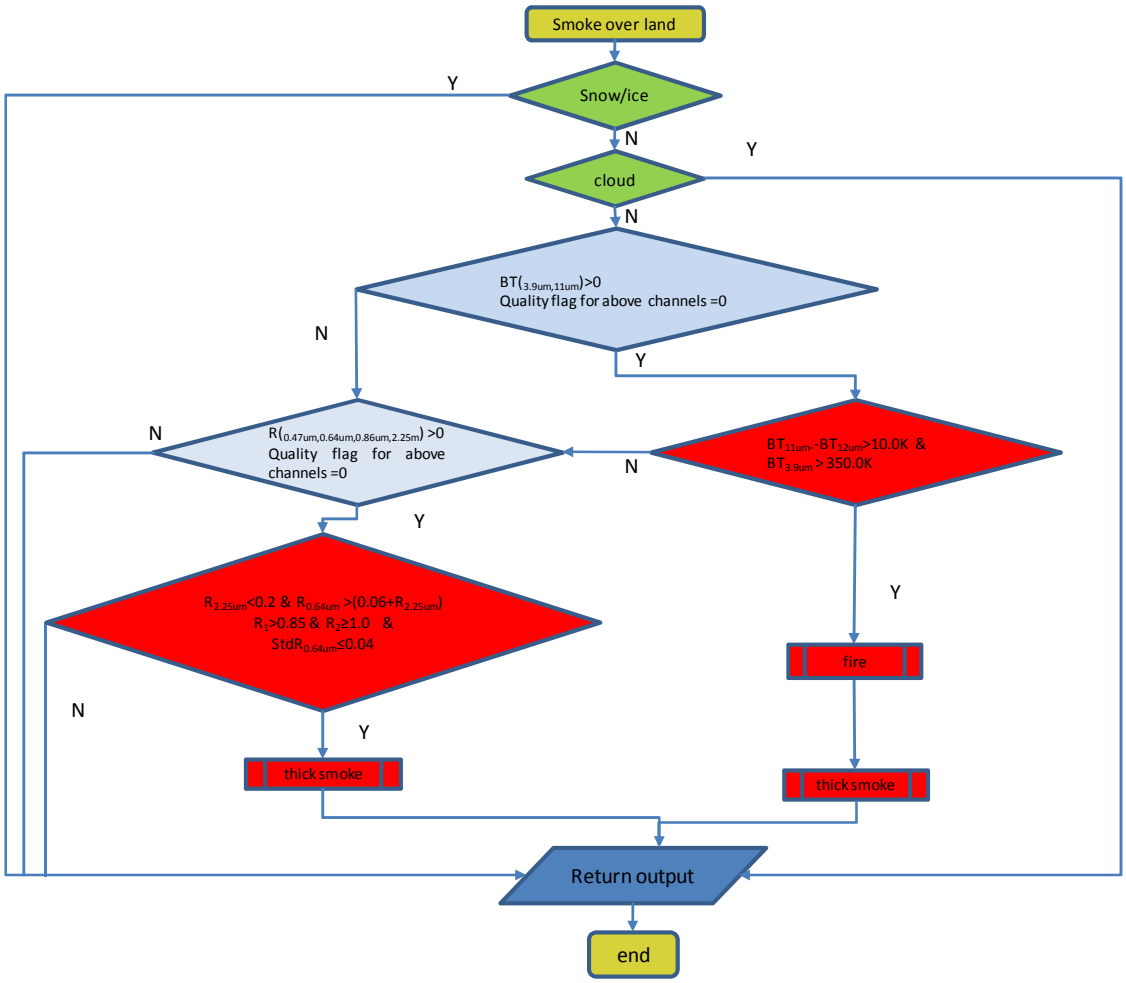


**Figure 12: Detailed flow chart of thick smoke detection over land.**

The specific tests as currently implemented sequentially are:

1) Test for the presence of snow/ice by first using ABI mask and then using internal snow/ice test. Also test for the presence of clouds by using ABI cloud mask. Pixel is considered to be obscured by clouds if ABI cloud mask tests in 3/7 (byte no./bit no.), 3/2, 2/5, 2(4)+ 3(3) is true. Any pixel with positive snow/ice/cloud mask is not processed.

2) Test for the quality of the input radiance data

   - $R_{0.47\mu m}$, $R_{0.64\mu m}$, $R_{0.86\mu m}$ , $R_{2.25\mu m} > 0$ &
   - $BT_{3.9\mu m}$, $BT_{11\mu m}$, > 0K
   - ABI quality flags for above channels equal to zero, indicating quality of the data is assured.

3) Fire detection (hot spot)
   If
   $BT_{3.9\mu m} > 350K$ and $BT_{3.9\mu m} - BT_{11\mu m} \geq 10K$
   then fire
4) Spectral and uniformity tests for thick smoke
   If
   $R_{2.25\mu m} < 0.2$ and
   $R_{0.64\mu m} > (0.06 + R_{2.25\mu m})$ and
   $R_1 \geq 0.85$ and $R_2 \geq 1.0$ and
   $StdR_{0.64\mu m} \leq 0.04$ (3x3)
   then thick smoke

5) Set smoke flag

   - If fire or thick smoke then smoke

#### 3.4.2.4.1 Example result

The results of an application of the smoke test to MODIS Terra data on May 2, 2007 at 16:35 UTC is shown in Figure 13. Smoke over Florida is detected. Comparisons of smoke mask to RGB images show that both smoke over land and water were well captured.

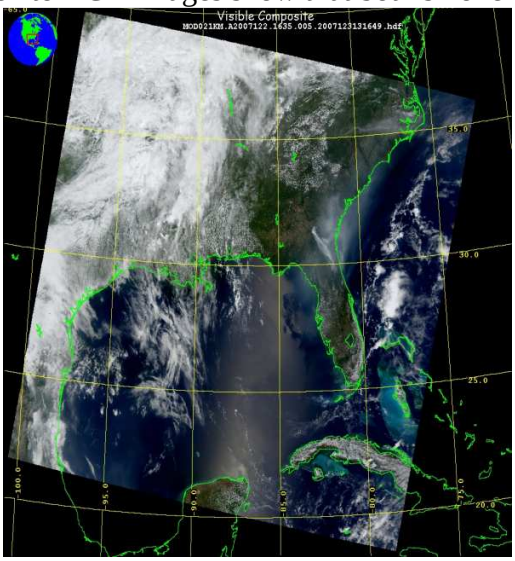


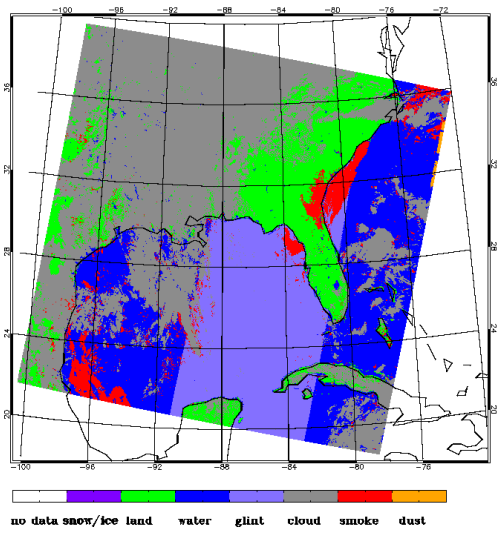


**Figure 13: Left: a red-green-blue (RGB) false color image of a MODIS Terra observation data on May 2, 2007 at approximate 16:35 UTC. . Right: the results of the smoke test where pixels flagged as smoky are red.**

### 3.4.2.5 Smoke detection over water

Figure 14 is a high level flow chart of the algorithm to detect the presence of smoke over water during daytime. The tests are not performed in the presence of ice clouds.

The specific tests as currently implemented sequentially are

1) Test for the presence of snow/ice by first using primary /secondary snow/ice mask. Also test for the presence of clouds by using ABI cloud mask. Pixel is considered to be obscured by clouds if ABI cloud mask tests in 3/7 (byte no./bit no.), 2/5, 2(4)+ 3(3) is true. Any pixel with positive snow/ice/cloud mask is not processed.

6) Test for the quality of the input radiance data

- $R_{0.47\mu m}$, $R_{0.64\mu m}$, $R_{0.86\mu m}$ , $R_{1.38\mu m}$ , $R_{2.25\mu m} > 0$

2) Uniformity test

If $StdR_{0.86\mu m}$ <=0.003 then
thin dust determination test
else
thick dust determination test

3.1) Thick dust determination test
If
$R_3 > 5.0$ and $R_{0.47\mu m} > 0.12$ and $0.022 < R_{1.61um} < 0.05$ and $R_4 \leq 0.5$
then thick dust
howver,
if $R_3 > 5.0$ then thin dust

3.2). thin smoke determination test

If $R_3 > 6.0$ and $R_4 \leq 0.3$ then thin dust

3) Set smoke flag

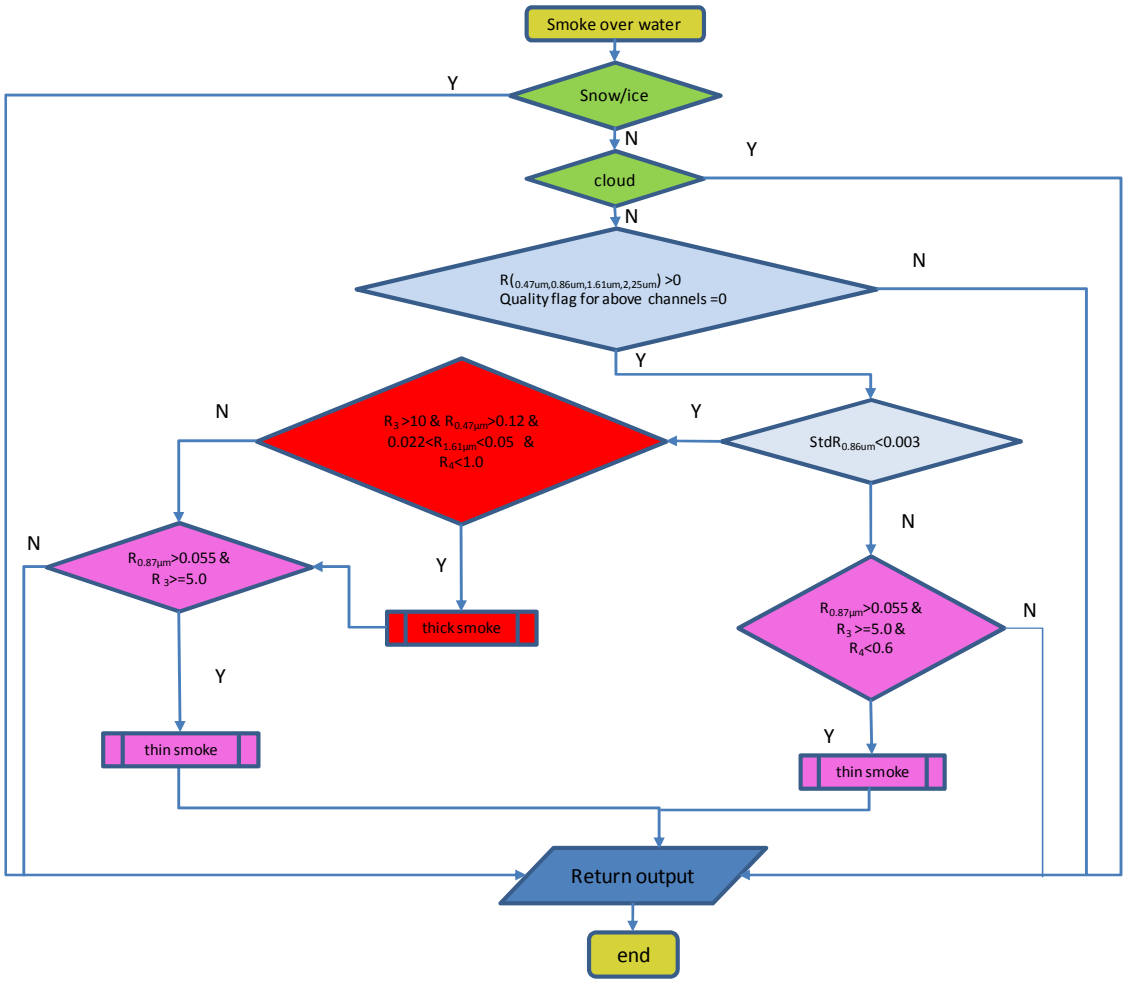


**Figure 14: Detailed flow chart of smoke detection over water.**

### 3.4.2.5.1 Example result

The results of an application of the smoke test to MODIS Terra data on October 28, 2003 at approximate 18:25 UTC is shown in Figure 15. Smoke over the coast of California due to a fire in the dry season is detected. The detected coverage of the smoke is very similar to the pattern that observed from the RGB image, indicating the success of ADP algorithm.

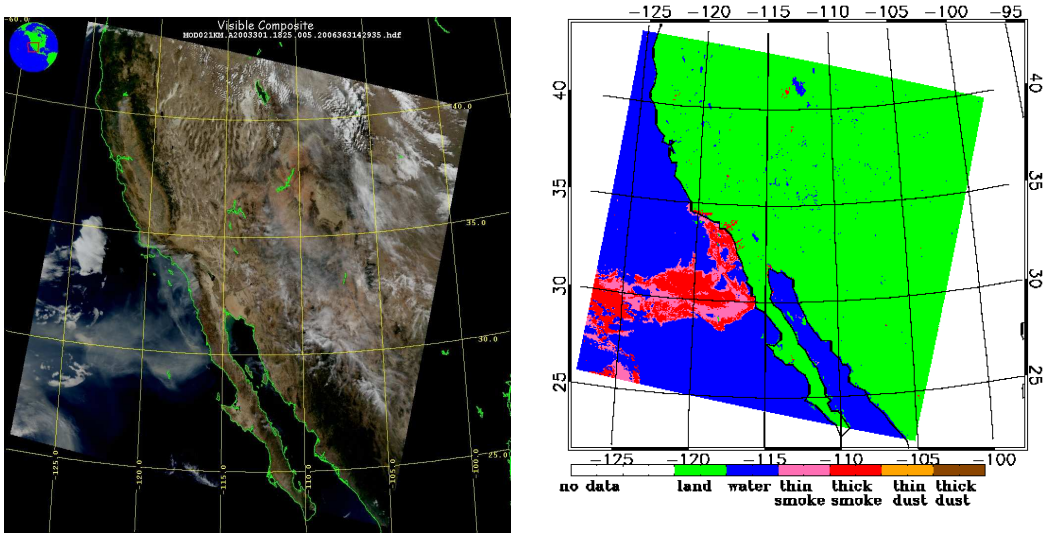


**Figure 15: Left: a red-green-blue (RGB) false color image of a MODIS Terra observation data on October 28, 2003 at approximate 18:25 UTC. Right: the results of ADP algorithm.**

### 3.4.3 Algorithm Output

The final output of this algorithm is a single yes/no mask for dust and smoke. The parameters are listed below in **Error! Reference source not found.**.

**Table 9 ABI aerosol imagery detection algorithm output**

| Name | Type | Description | Dimension |
|---|---|---|---|
| Aerosol flag | output | Detected aerosol binary flag (1/0 - yes/no) | grid (xsize, ysize) |
| Smoke flag | output | Detected smoke binary flag (1/0 – yes/no) | grid (xsize, ysize) |
| Dust flag | output | Detected dust binary flag (1/0 – yes/no) | grid (xsize, ysize) |
| quality flag for smoke | output | Smoke detection quality flag (0/1 – good/bad ) | grid (xsize, ysize) |
| quality flag for dust | output | Dust detection quality flag (0/1 – good/bad ) | grid (xsize, ysize) |

In addition the following information is included in the output:

- Date and Time (swath beginning and swath end)
- Bounding Box
  - product resolution (nominal and/or at nadir)
  - number of rows
  - number of columns
  - bytes per pixel
  - data type
  - byte order information
  - location of box relative to nadir (pixel space)
- Product Name

- Product Units
- Ancillary Data to Produce Product (including product precedence and interval between datasets is applicable)
    - Version Number
    - Origin (where it was produced)
    - Name
- Satellite
- Instrument
- Altitude
- Nadir pixel in the fixed grid
- Attitude
- Latitude
- Longitude
- Grid Projection
- Type of Scan
- Product Version Number
- Data compression type
- Location of production
- Citations to Documents
- Contact Information

# 4 Test Datasets and Outputs

## 4.1 Proxy Input Data Sets and validation data

### 4.1.1 Input Data sets

The MODIS instrument flying on NASA's Aqua and Terra satellites measures radiances at 36 wavelengths including infrared and visible bands with spatial resolution 250m to 1km. The cloud mask is part of the MODIS Cloud Product [*Ackerman et al.*, 1998, 2008; *Frey et al.*, 2008; *King et al.*, 2003; *Platnick et al.*, 2003]. Due to the fact that MODIS has nearly all ABI channels, currently MODIS provides the optimum source of data for testing (Table 10)

**Table 10 Mapping of ABI Channels to MODIS Channels**

| ABI Channel (μm) | MODIS Channel (μm) |
|---|---|
| Channel 1: 0.45 - 0.49 | Channel 3: 0.459 - 0.479 |
| Channel 2: 0.59 - 0.69 | Channel 1: 0.62 - 0.67 |
| Channel 3: 0.846 - 0.885 | Channel 2: 0.841 - 0.876 |
| Channel 4: 1.371 - 1.386 | Channel 26:1.36 - 1.39 |
| Channel 5: 1.58 - 1.64 | Channel 6: 1.628 - 1.652 |
| Channel 6: 2.225 - 2.275 | Channel 7: 2.105 - 2.155 |
| Channel 7: 3.8 – 4.0 | Channel 21: 3.929 – 2.989 |
| Channel 11: 8.3 – 8.7 | Channel 29: 8.4 – 8.7 |
| Channel 14: 10.8 – 11.6 | Channel 31: 10.78 – 11.28 |
| Channel 15: 11.8 – 12.8 | Channel 32: 11.77 – 12.27 |

The disadvantage is in the lack of temporal coverage. In the current algorithm (V5) testing, a total of 146 cases (or MODIS granules) (80 for dust and 66 for smoke) were used for testing the performance of ADP algorithm. Currently, no simulated ABI data with aerosols are available but we plan to use the simulated ABI data once it becomes available.

MODIS L1-B 1km radiance data were obtained from NASA Level 1 and Atmosphere Archive and Distribution System (LAADS, http://ladsweb.nascom.nasa.gov/). Visible channel reflectances were normalized to the overhead sun position by dividing with the solar zenith angle. For the IR channels, radiances were converted to Brightness Temperatures. Viewing and illumination geometry and geo-location are from MOD/MYD03. Various cloud tests used in ADP are extracted from the corresponding bits in the MODIS cloud mask product (MOD/MYD35). Snow/ice mask from MOD/MYD35 is used as the primary source of snow/ice mask. Land/water mask is also from MOD/MYD35. Both sun glint mask and day/night flag are internally calculated as described in section 3.12.

### 4.1.2 Truth data

,

#### 4.1.2.1 Supervised MODIS RGB image and MODIS Aerosol optical depth product

Both smoke and dust have a distinctive signature in RGB image, and NASA Natural Hazard system (http://earthobservatory.nasa.gov/NaturalHazards/) and MODIS rapid response system (http://rapidfire.sci.gsfc.nasa.gov/gallery/) routinely issues MODIS observations containing the smoke and dust outbreaks around the globe. By selecting granules which are dominated by either only smoke or only dust, a supervised truth

dataset were obtained. Then the corresponding Aerosol Optical Depth (AOD) product is used to identify the smoke/dust laden (AOD>0.2) and smoke/dust free (0.2>AOD>0.0) pixels; Note that, the traditional MODIS AOD product over land only covers dark dense vegetation surface. However, MODIS deep blue AOD product on AQUA provides AOD coverage on bright surface such as over desert. MODIS pixels with no AOD retrievals are considered as covered by clouds or snow/ice, bright surface over land and bad input data. These conditions are consistently unfavorable for detection of smoke/dust as well as discussed in Section 3. In addition, due to the difference in cloud screening procedures between MODIS AOD product and ADP algorithm, only pixels with both MODIS AOD product and ADP indicating cloud-free conditions are used for quantitative analysis.

#### 4.1.2.2 CALIPSO VFM product

With the launch of CALIPSO and CloudSat in the EOS A-Train formation in April 2006, the ability to conduct global satellite cloud product validation increased significantly. Besides cloud type, CALIPSO also identifies aerosol types including smoke and dust. Vertical Feature Mask (VFM) is the CALIPSO product which is used for validating ABI ADP product. It gives not only vertical distribution of aerosol layer but also 6 types of aerosol, including clean marine, dust, polluted dust, polluted continental, clean continental, polluted dust and smoke. However, the sparse spatial coverage and narrow swath of CALIPSO lidar observation limits the amount of match-up overpasses with MODIS for smoke and dust cases. From 2006 to 2010, about 48 match-up cases are found with CALIPSO passing through the smoke/dust plume. Among them there are 22 smoke cases and 26 dust cases.

## 4.2. Output from simulated/proxy data sets

### 4.2.1. Output for Dust Detection

#### 4.2.1.1. Comparison with RGB image and AOT product

Supervised RGB image can capture dust events very well since dust plumes look brown in the image compared to cloud. Thus, RGB image can be used to validate the ADP dust detection algorithm. Therefore, we can apply dust detection algorithm to MODIS measurement of a dust event and compare the detection result with the MODIS RGB image. One example is shown in Figure 16 for the MODIS Terra image of April 7, 2007 at 07:30UTC. Qualitative comparison of dust detection with MODIS RGB image shows a good agreement.

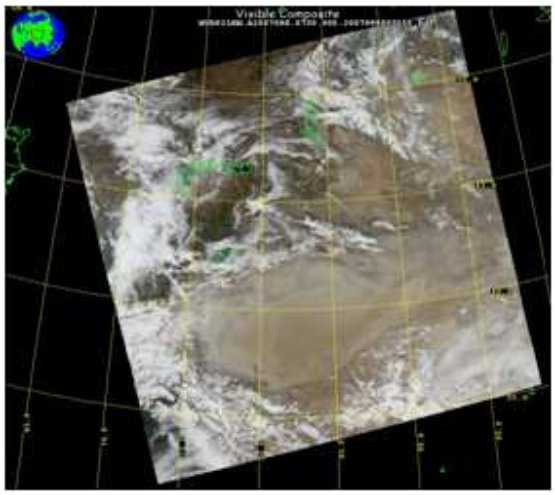

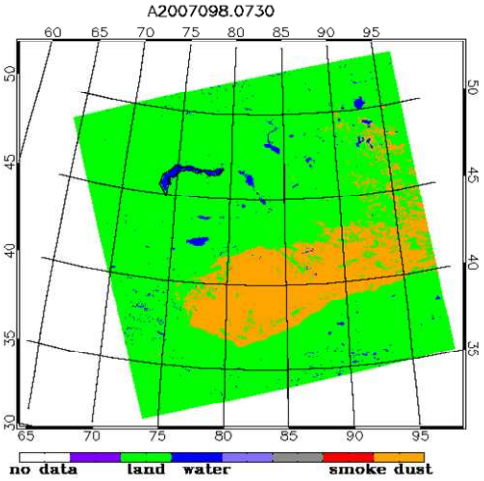


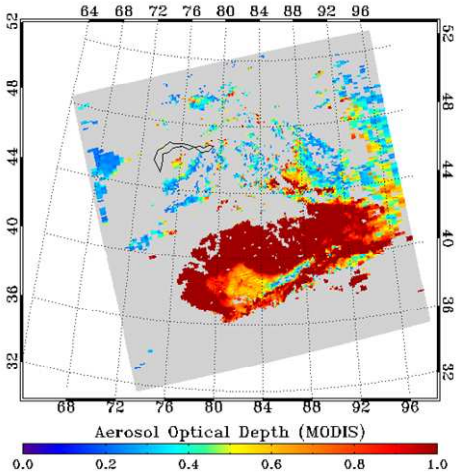


**Figure 16: Left: MODIS Terra RGB Image on April 7, 2007 at about 07:30 UTC. Right: the results of the dust detection. Bottom: MODIS AOD (only pixels with AOD > 0.2 are shown)**

Dust particles are mainly located near desert regions and downwind areas and a dust event is mainly associated with high aerosol optical depth (AOD) so that the AOD distribution retrieved from satellite observation can help us to qualitatively examine the ADP dust detection algorithm.

### 4.2.1.2. Comparison with CALIPSO VFM

CALIPSO is onboard the same spacecraft as MODIS Aqua and its VFM products provide vertical distribution of 6 aerosol types, including smoke and dust over its narrow (about 5 km) track. Although the sparse spatial coverage of CALIPSO lidar observations limits the number of overpass matchups with MODIS Aqua granule, several cases containing dust outbreak were found. And the possibility of using the MODIS and CALIPSO overpass and the CALIPSO aerosol type data to validate the ADP dust detection is explored.

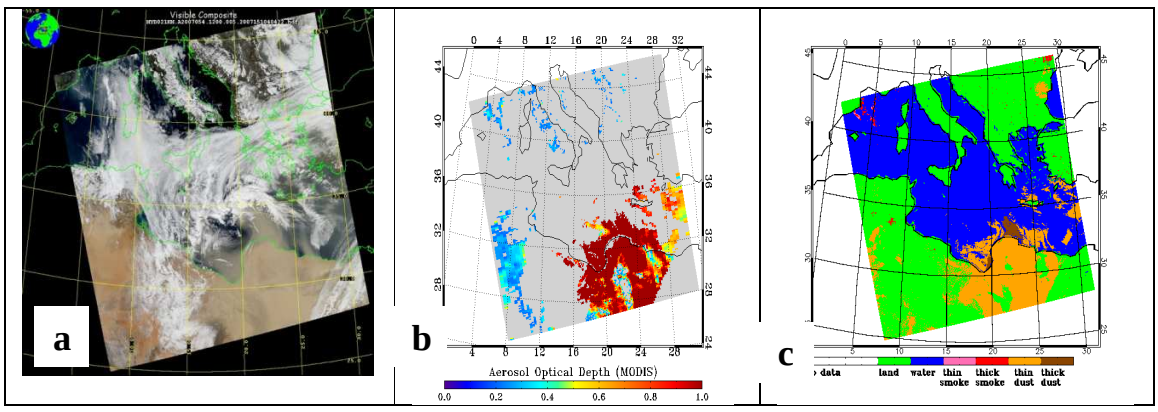

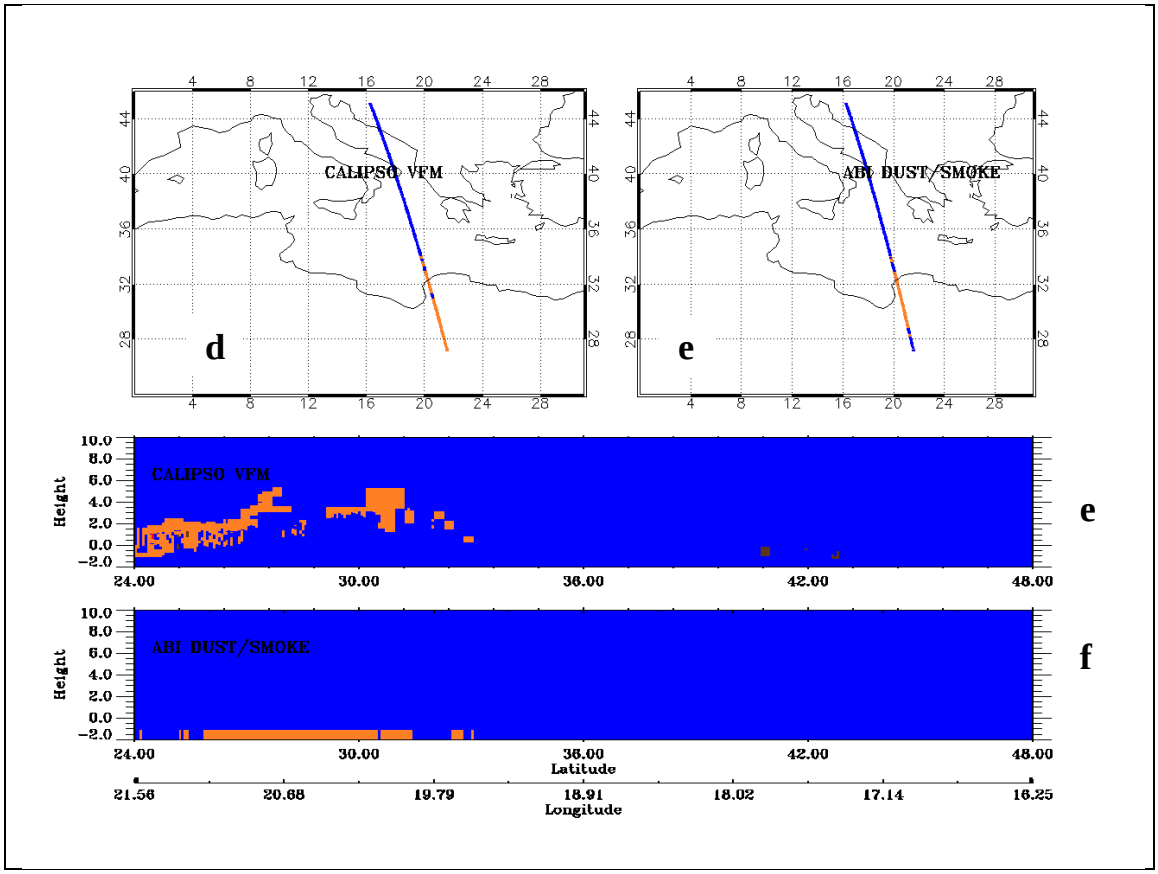


**Figure 17: Comparison of dust detected (orange) using ABI ADP algorithm with CALIPSO Vertical Feature Mask (VFM) on February 23, 2007, UTC 12:00. a) RGB image, b) Aerosol Optical depth from MODIS C5 aerosol Product, c) Dust mask from ADP, d) Dust (orange) on CALIPSO track, e) Dust (orange) detected with ABI ADP algorithm on CALIPSO track, f) Dust vertical distribution on the part of CALIPSO track collocated with ABI ADP, g) Dust from ABI ADP on the same part of track as in b.**

First example is shown in Figure 17 for CALIPSO VFM vs. ABI ADP for MODIS Aqua image of February 23, 2007 at 12:00UTC. The dust plume is clearly visible in the RGB image. As shown in Figure 17 (d) and (e) CALIPSO VFM indicates existence of dust over the beginning part of CALIPSO track which has collocations with MODIS, and the dust is seen starting from the surface of Libyan Desert and becoming elevated over the sea. ABI ADP dust mask over the co-located CALIPSO track is given in Figure 17c. CALIPSO VFM data shows that dust was dispersed between the surface and 2 km (Figure 17g). First of all, it is clearly seen that there is a good agreement between the dust plume pattern detected by ADP and the pattern shown in both RGB and MODIS AOD. Secondly, similar good agreement is also seen on CALIPSO VFM track. According to the definition of accuracy (correct aerosol detection) shown in equation in 4.31, the agreement between ABI ADP and CALIPSO VFM is 85%.

**Figure 18: Comparison of dust detected (orange) using ABI ADP algorithm with dust (orange) and polluted dust (brown) in CALIPSO Vertical Feature Mask (VFM) on May 09, 2007 at UTC 14:55. a) RGB image, b) Aerosol Optical depth from MODIS C5 aerosol Product, c) Dust (orange) on CALIPSO track, d) Dust (orange) detected with ABI ADP algorithm on CALIPSO track, e) Dust vertical distribution on the part of CALIPSO track collocated with ABI ADP, f) Dust from ABI ADP on the same part of track as in b.**

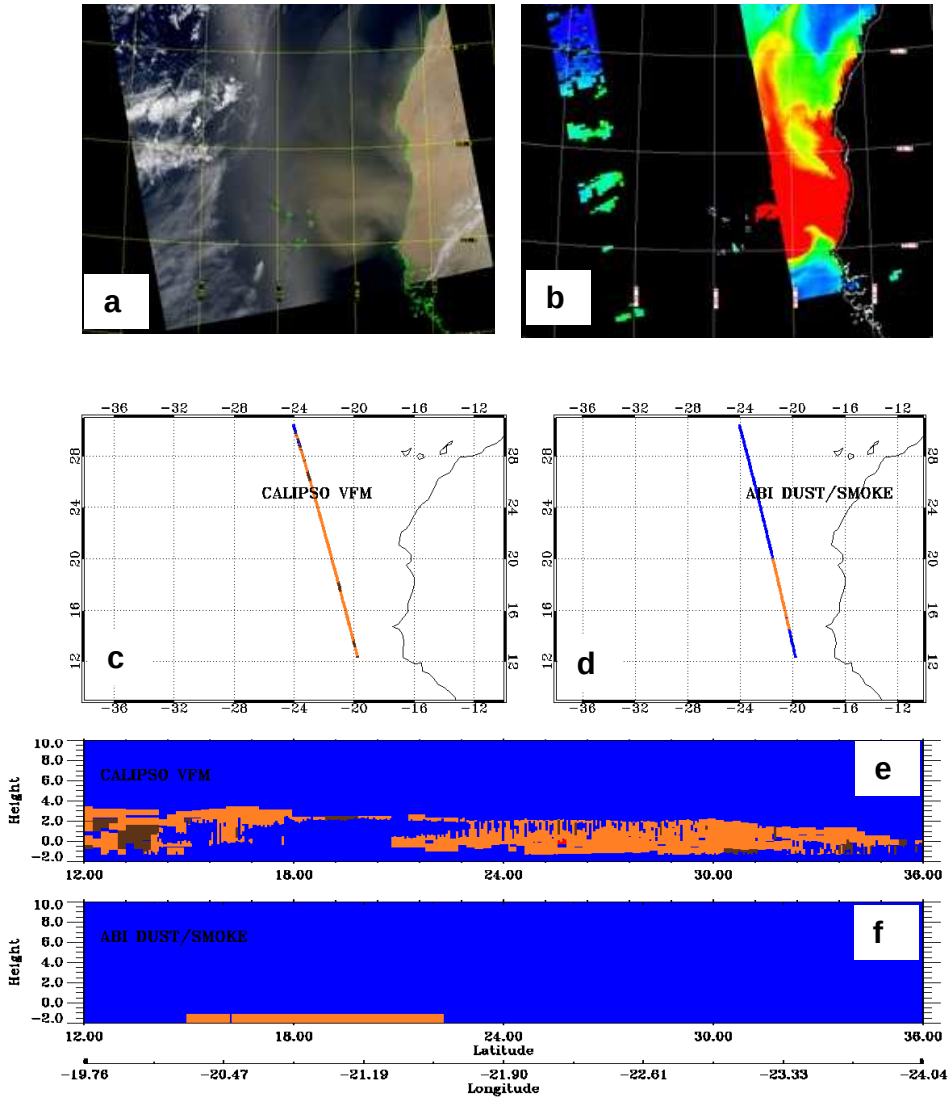


Unlike the case in Figure 17, the co-located overpass shown in Figure 18 between CALIPSO and MODIS is over water. It is noted that this co-located overpass is right on the edge of a sun glint region where ABI ADP data are not processed. Therefore, by excluding pixels in the overpass within sun glint and with MODIS AOD less than 0.2, the agreement between ABI ADP and CALIPSO VFM is about 81 %. For a total of 26 match-up cases for dust, the average of agreement is ~81%.

### 4.2.2. Output for Smoke Detection

## 4.2.2.1. Comparison with RGB image

Smoke is associated with fire events and the spatial distribution of smoke plume is uniform and looks gray to a human eye compared to a cloud. This feature is useful in identifying smoke plumes in a RGB image without difficulty. Thus, RGB image can be used to validate the ADP smoke detection. One example is shown in **Error! Reference source not found.** for a fire event in Australia observed by MODIS Aqua on August 25, 2006 at 17:15UTC. Qualitative comparison of smoke detection with MODIS RGB image shows a good agreement, especially for the thick smoke plumes over vegetated areas.

**Figure 19: Left: MODIS Aqua RGB Image on August 25, 2006 at 17:15UTC. Right: the results of the smoke detection (pixels flagged as smoky are in colored red). Bottom: MODIS AOD (only larger than 0.2 are shown).**

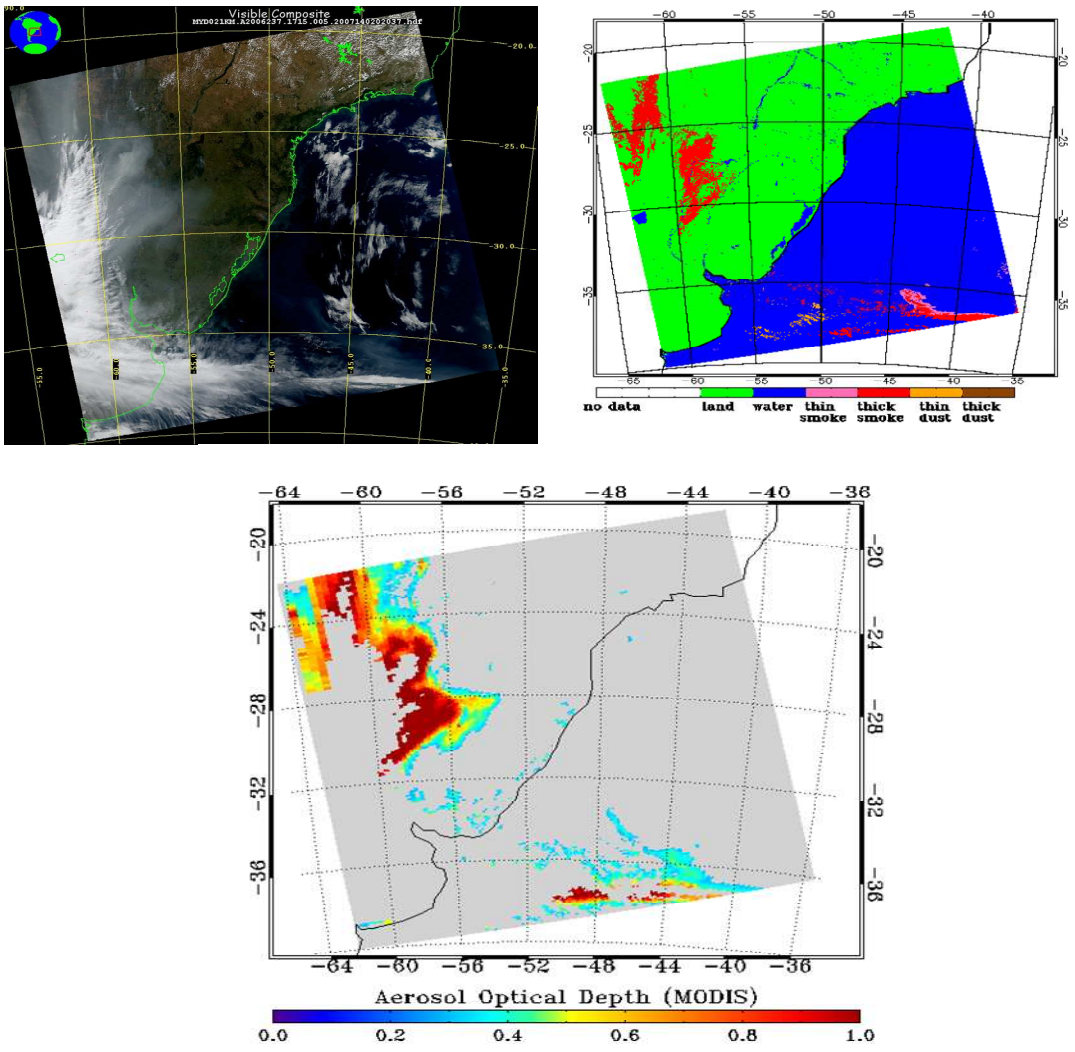


In general, aerosol optical thickness of smoke (shown in Figure 19) is high and its spatial distribution is in plume structure. Thus, AOD image can be used to quantitatively

validate our ADP smoke detection. As seen in Figure 19, AOD plumes compare well with the ADP smoke flags. The agreement is 84%.

### 4.2.2.2. Comparison with CALIPSO VFM

In figures 20 and 21, two cases of ABI smoke detection is shown for two different days in different years. For both examples shown, ABI smoke detection mask agrees well with MODIS RGB image and the matchups with CALIPSO track show that the agreement between what CALIPSO observed and what ABI is showing is good. Parts of the track where CALIPSO detects smoke, ABI identifies those pixels as clear-sky/clouds or the other way. It should be noted that we have not yet tested the sensitivity of our retrieval to the height of the aerosol layer and aerosol amount. Although, we can use CALIPSO to identify the height of the aerosol, we have not taken the validation efforts to the next level where we will be conducting "deep-dive" studies of individual case studies to understand the limitations of the algorithms.

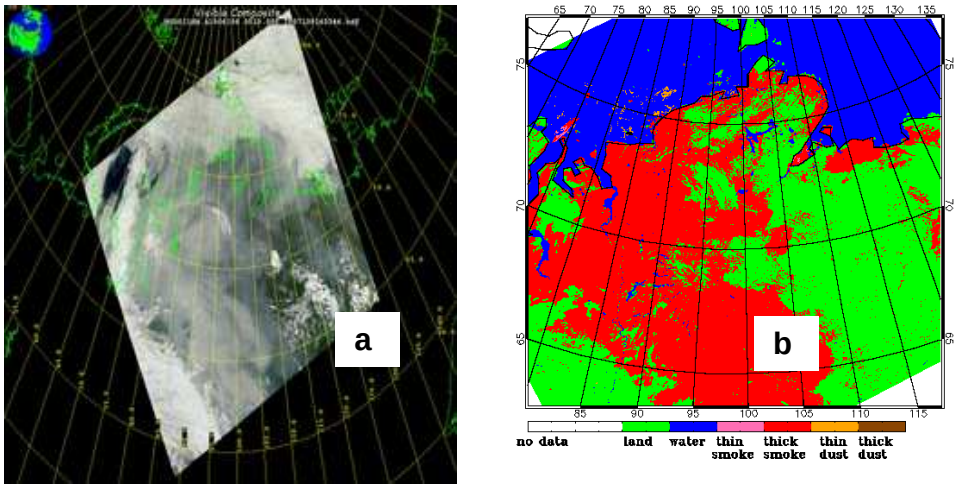

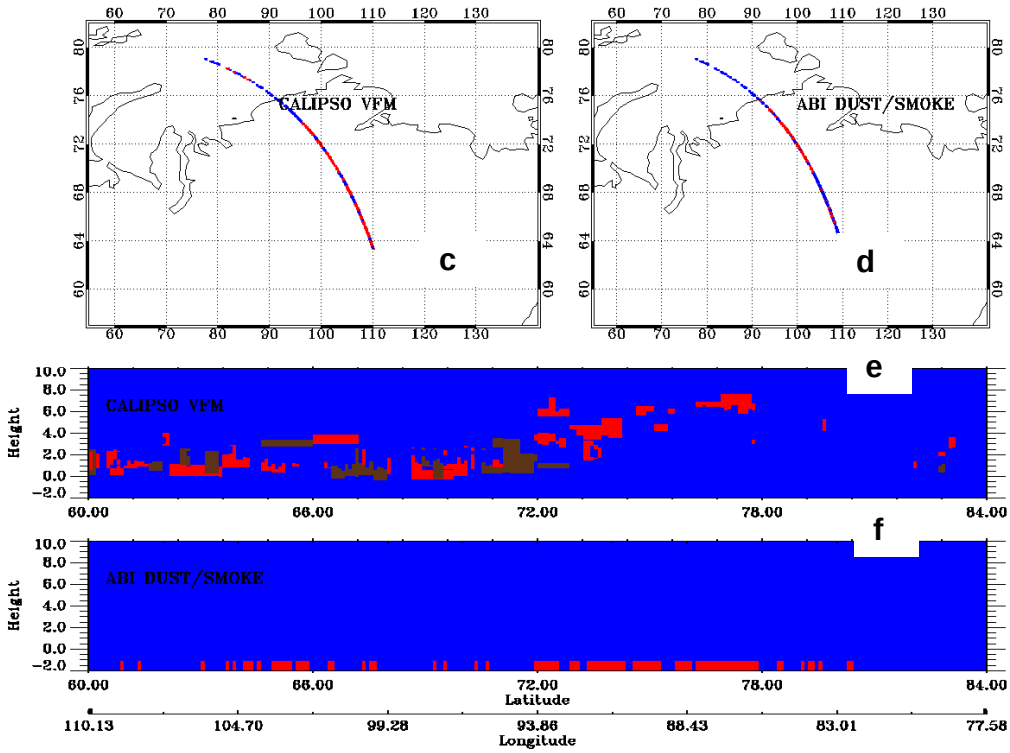


**Figure 20: Comparison of smoke detected (red)) using ABI ADP algorithm with smoke in CALIPSO Vertical Feature Mask (VFM) on July 25, 2006, UTC 05:15. a. RGB image b. Aerosol Optical depth from MODIS C5 aerosol Product. C. Smoke (red) on CALIPSO track. d. Smoke detected with ABI ADP algorithm on CALIPSO track. e. Smoke vertical distribution on the part of CALIPSO track collocated with ABI ADP d. smoke from ABI ADP on the same part of track as in b.**

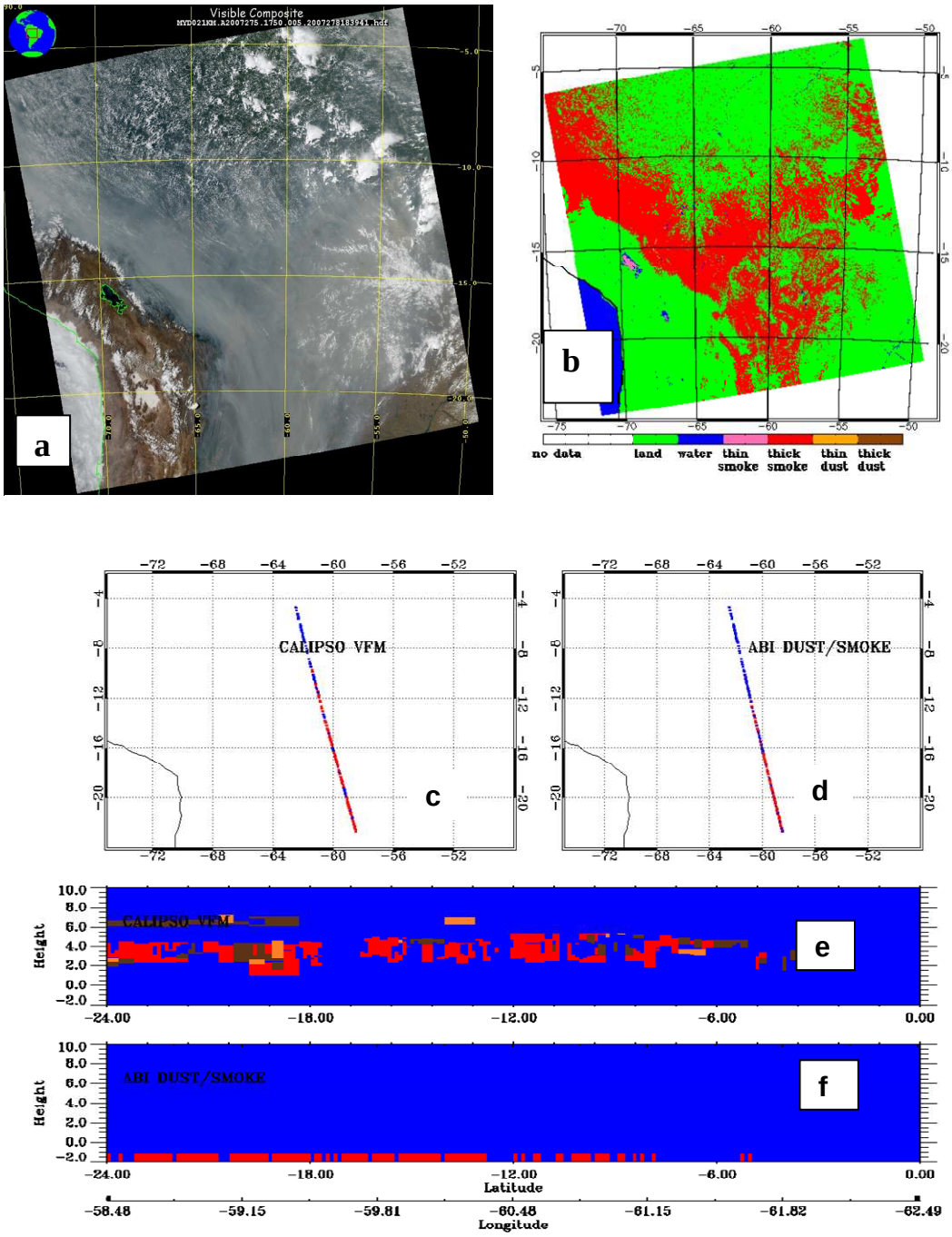


**Figure 21: Comparison of smoke detected (red) using ABI ADP algorithm with smoke in CALIPSO Vertical Feature Mask (VFM) on October 2, 2007 at 17:50 UTC. a) RGB image, b) Aerosol Optical depth from MODIS C5 aerosol Product, c) Smoke (red) on CALIPSO track, d) Smoke detected with ABI ADP algorithm on CALIPSO track, e) Smoke vertical distribution on the part of CALIPSO track collocated with ABI ADP, d) smoke from ABI ADP on the same part of track as in b.**

For smoke detection, two CALIPSO VFM vs. ABI ADP cases are presented. They are both over land on July 23, 2006 at 05:15 UTC and October 2, 2007 at 17:50 UTC (**Error! Reference source not found.**and **Error! Reference source not found.**). The agreement between the ABI ADP and CALIPSO VFM is 75% and 80% respectively. For a total of 22 smoke cases, the agreement between ABI ADP and CALIPSO VFM is about 80%.

### 4.2.3. Correct Detection (Accuracy) Estimates

Due to lack of ground truth for the accuracy estimate, the evaluation of ADP products is mainly based on the inter-comparison to other satellite based smoke and dust products (such as RGB image, HMS smoke analysis, and CALIPSO VFM product). As mentioned before, the correct detection estimates are semi-quantitative.

Correct detection = (TPD + TND) / (TPD+FPD+TND+FND) (4.3.1)

In equation 4.3.1, TPD is true positive detection, TND is true negative detection, FPD is false positive detection, and FND is false negative detection. The primary validation approach will provide an overall performance of the algorithm but will not provide information on performance of the algorithm over different geographic regions. Therefore, additional spot checks and statistics will be carried out.

Because accuracy of aerosol detection calculated using equation 4.3.1 will include true negative detects (clear sky pixels), it will not provide information on the true positive detects which a user might be interested in. Therefore, probability of detection and false alarm ratio (FAR) are computed using equations 4.3.2 and 4.3.3:

$$POD = \frac{(TPD)}{(TPD+FND)} * 100 \quad (4.3.2)$$

$$FAR = \frac{(FPD)}{(FPD+TPD)} * 100 \quad (4.3.3)$$

As discussed in section 4.2, two types of truth data are used. One is the supervised MODIS RGB and MODIS AOD products and the other one is CALIPSO VFM product. By collocating outputs from ABI ADP algorithm run with MODIS measured radiance as proxy with these two types of truth data, statistics on accuracy, hit rate, and miss rate are calculated (see 1)

**Table 11 Correct Detection, Probability of Detection, and False Alarm Ratio of ABI dust and smoke detection**

| | No. of Matchups | Correct Detection | POD | FAR |
|---|---|---|---|---|
| | CALIPSO VFM | | | |
| Dust | 2031 (26) | 81.3% | 70.6% | 29.4% |
| Smoke | 5192 (22) | 80.5% | 71.9% | 28.1% |
| | Supervised MODIS AOD product | | | |
| Dust over land | 688911 (54) | 84.5% | 63.6% | 36.3% |
| Dust over water | 353723 (45) | 83.2% | 78.5% | 21.5% |
| Smoke over land | 639637 (60) | 80.1% | 77.3% | 22.7% |
| Smoke over water | 459803 (57) | 82.2% | 86.4 % | 13.5% |

Based on these validation studies, the GOES-R ABI aerosol detection algorithm meets the Functional Product and System requirements (80% correct detection for dust over land and water, for smoke over land, and 70% correct detection for smoke over water).

However, we are increasing our validation efforts by compiling large amount of AOD and extinction data from ground-based networks such as AERONET (AERosol Robotic NETwork) and IMPROVE (Interagency Monitoring of Protected Visual Environments). The presence of dust and smoke can be indirectly inferred from these measurements and used in the validation of the ABI aerosol dust/smoke detection product. This work is currently ongoing and will be presented in any subsequent documents related to validation are presented.

## 4.3. Error Budget

To examine the sensitivity of the detection algorithm to the radiometric bias/noise, we perturbed the reflectances at all detection channels with a bias of -5% and a random noise of 5% and compared the results with those without the radiometric perturbation. An

example of a dust case for the MODIS Aqua data on April 15, 2003 at 20:20 UTC is shown in ***Figure 22***. After adding the radiometric noise/bias, the number of dust pixels detected is reduced by about 9.3%.

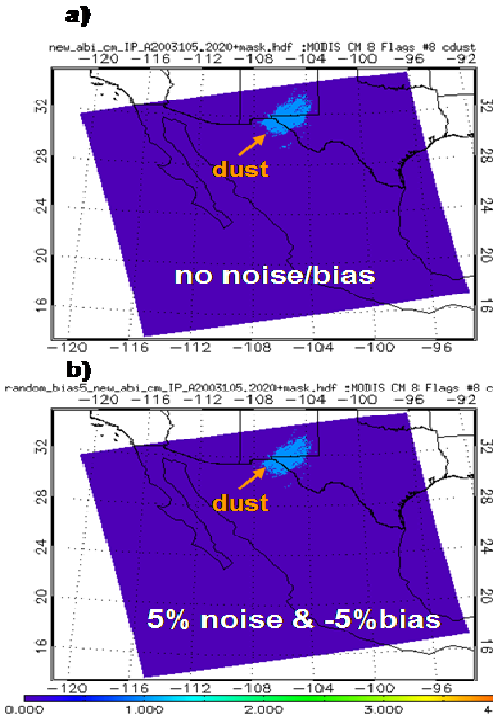


**Figure 22: Comparison of dust detection before (a) and after (b) the perturbation on the reflectance of the detection channels for a dust case. c) Scatter plot of the detection results before and after the perturbation of 5% noise and -5% biases. Linear regression line (red color) and the formula are given. The blue envelope is the ±18% ABI requirement. d) Similar to c) but only 5% noise perturbation is applied.**

An example of smoke case for the MODIS Aqua data on August 19, 2003 at 19:00 UTC is shown in Figure 23. After adding the radiometric noise/bias, the number of dust pixels detected is reduced by about 7.6%. The impact mainly comes from the bias rather than the noise. These sensitivity tests suggest that algorithm modifications may be needed after the ABI instrument launches or instrument behavior changes from pre-launch to post-launch.

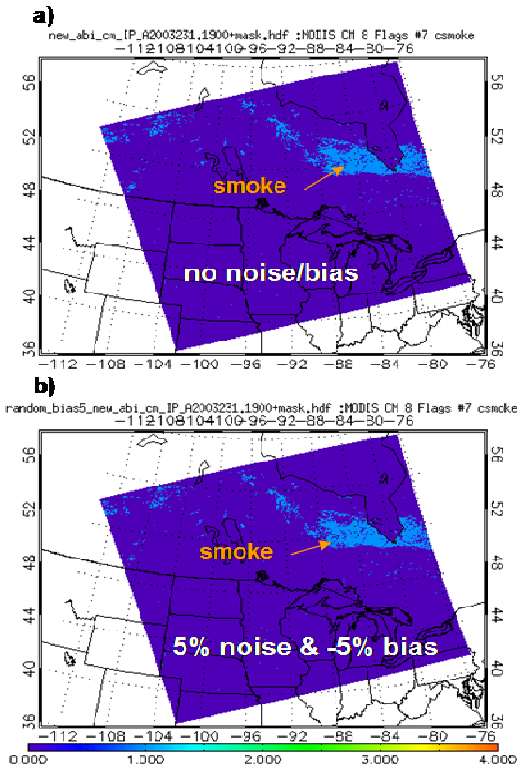


**Figure 23: Similar to Figure 22 but for a smoke case of MODIS Aqua data on August 19, 2003 at approximate 19:00 UTC.**

## 4.4. Framework run and validation

### 4.4.3. Framework run

As shown in section 4.1, the ADP algorithm was validated extensively. However, this validation work was done with offline runs, i.e., running ADP algorithm without integrating it into GOES-R ABI product framework. Under the operational environment, ADP algorithm will be running in the framework. In general, the procedure for running the ADP algorithm in the framework is as follows: first, common input radiance data are generated from proxy data set, the common dataset includes both the required input and ancillary data in a common data format, i.e., netCDF. Second, the aerosol detection algorithm is called according to the order of precedence. Finally, results from each product are written to an output file in netCDF format.

### 4.4.4. Consistency tests with MODIS granules

To test the offline runs with runs through integration of ADP algorithm into the framework, comparisons were made between outputs from offline run with outputs from framework run with common input data and using the V3 algorithm. For tests shown below, MODIS observations from two granules were used as proxy for GOES-R ABI, i.e., 1 km radiances from MODIS bands corresponding to ABI channels required by ADP

algorithm and cloud mask from MODIS cloud mask product. Figure 24 and Figure 25 show the comparisons of offline smoke/dust mask with those from framework run for two MODIS granules. Framework run was able to reproduce exactly the same results as from offline run for one granule and another one except one pixel. The difference in that one pixel is caused by the difference of precision in one of the threshold values used in the algorithm, i.e., brightness temperature of MODIS band 31 (11μm, BT11). The value of BT11 is 284.99874 in offline run and 285.000122 in framework run, while the threshold used in the smoke detection is set as 285.0.

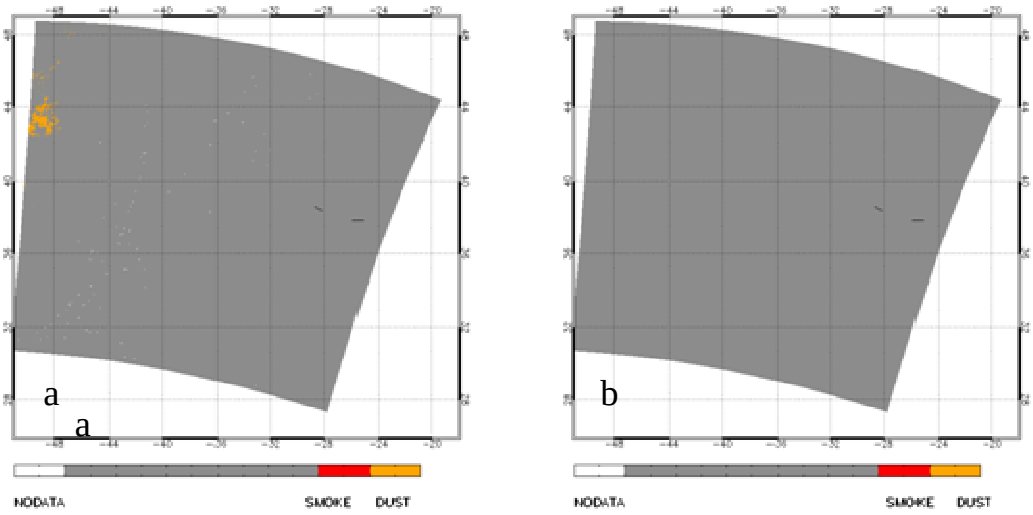


**Figure 24: Comparison of offline run with framework run for MODIS (Terra) observation on June 4, 2005, UTC13:20. a) smoke/dust mask from framework run, b) difference between framework run and offline run.**

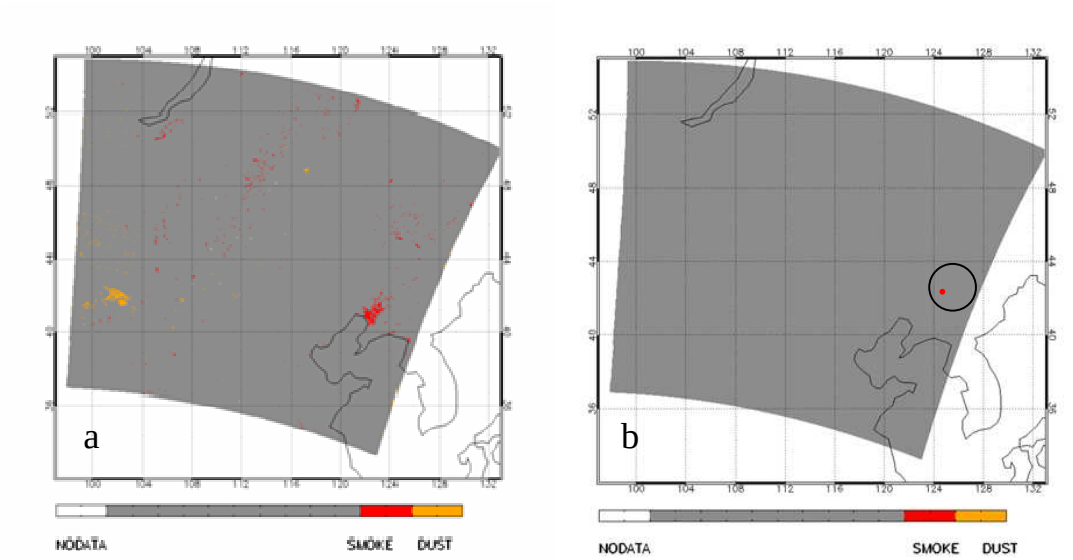


**Figure 25: Comparison of offline run with framework run for MODIS (Terra) observation on June 4, 2005, UTC03:25. a) smoke/dust mask from framework run, b) difference between framework and offline run.**

### 4.4.5. Results from Framework run with global MODIS observation

To further test the framework run, global MODIS (Both Terra and Aqua) observations for August 24 and 25, 2006 were selected as proxy input to run ADP algorithm in the framework. Figure 26 ***a-b*** show global smoke/dust mask product from framework run of the ADP algorithm. Note that, the white shaded region is due to the missing MODIS granule data. In general, the framework run produced no abnormal smoke or dust pattern for each of these two days, and consistency is seen between results from these two consecutive days. Furthermore, large smoke plume resulting from biomass burning were identified over South America, and dusts from dust storm are shown over Sahara desert. Although the location of the dust and smoke plumes are consistent between the two days, there are differences in the amount of smoke and dust present. This is very typical because while old fires die out, new fires form and dust transport occurs in the free troposphere moving it long distance over short time periods. In fact, with the current operational GOES fire and aerosol products, we know that substantial diurnal variation exists for fire duration. In addition, as shown in Figure 27 and Figure 28 for smoke and dust case, smoke/dust mask produced by ADP from framework run has very similar pattern of smoke/dust as identified in MODIS RGB images. These framework runs were not compared to offline runs. It should also be noted that these runs are based on Version 3 algorithm. Framework runs using Version 5 algorithm for a longer time period covering several seasons is currently underway. Results are not available yet to present in the ATBD.

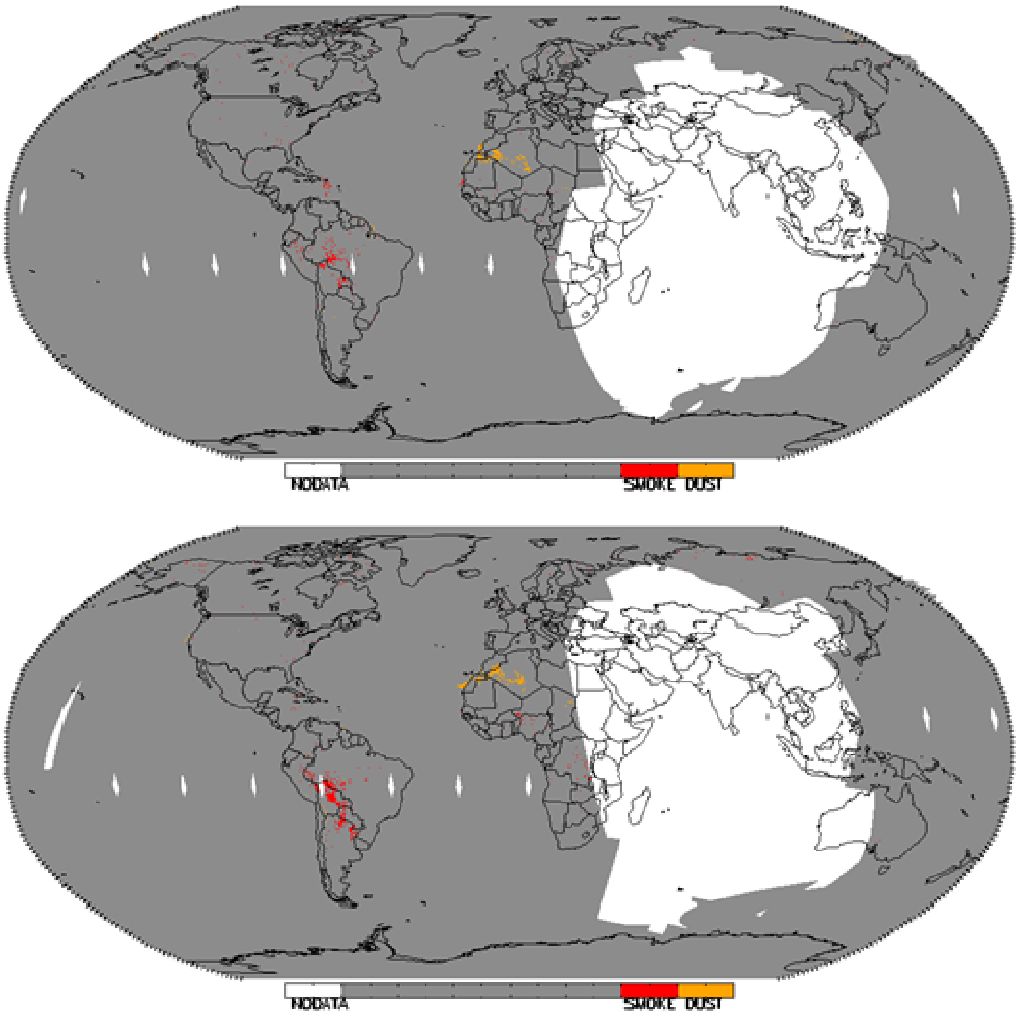


**Figure 26: Global smoke/dust mask from ADP algorithm run in the framework for MODIS (Aqua) observations. a) August 24, 2006, b) August 25, 2006.**

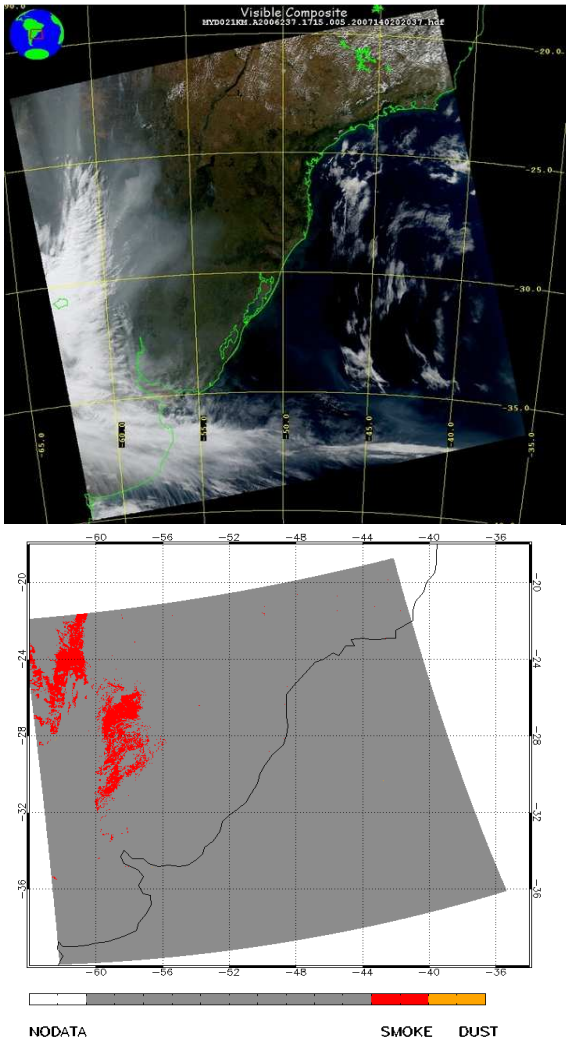


**Figure 27: Smoke/dust mask from ADP algorithm run in the framework for Aqua, August 27, 2006, UTC 17:15. Left: MODIS RGB image Right: smoke/dust mask from ADP.**

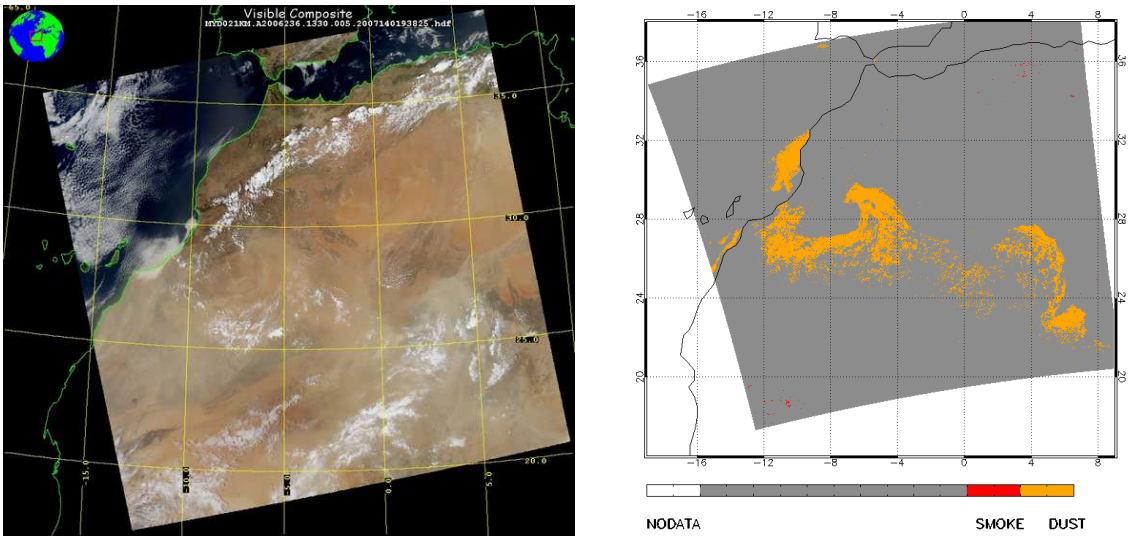


**Figure 28: Smoke/dust mask from ADP algorithm run in the framework for Aqua, August 24, 2006, UTC 13:20. Left: MODIS RGB image Right: smoke/dust mask from ADP.**

# 5. PRACTICAL CONSIDERATIONS

## 5.2. Numerical Computation Considerations

The ADP algorithm is implemented sequentially. Because some tests require ancillary data, the ancillary data (e.g., day/night, snow/ice, sun glint, and cloud/clear) need to be input first. To balance the efficiency and memory requirement for the full disk processing, a block of scanning pixels are read into a RAM buffer together instead of reading data pixel by pixel.

## 5.3. Programming and Procedural Considerations

The ADP requires knowledge of spatial uniformity metrics that are computed for each pixel using pixels that surround it. Detection is performed separately for land and water. In addition, future temporal tests require information from the previous image. Beyond this reliance, the ADP is a pixel by pixel algorithm.

## 5.4. Quality Assessment and Diagnostics

The following procedures are recommended for diagnosing the performance of the ADP.

- Monitor the percentage of pixels falling into each ADP aerosol bin values. These values should be quasi-constant over a large area.

- Monitor frequency of false positives of regions to assess need to have region specific thresholds developed and implemented.
- Periodically image the individual test results to look for artifacts or non-physical behaviors.
- Monitor retrievals over different surface (geographic) type for dependency of errors on surface brightness
- Monitor spectral threshold values and provide a quality flag depending on how close the spectral BT differences are to specified thresholds
- Monitor retrievals for temporal consistency. Are retrievals consistent from image to image?

Qualify flag with value of 0/1/2 representing lower/medium/high confidence will be generated according to how far the actual value for each test is from the predefined threshold.

## 5.5. Exception Handling

The quality control flags for ABI ADP will be checked and inherited from the flagged Level 1b sensor input data, including bad sensor input data, missing sensor input data and validity of each channel used; and will also be checked and inherited from the ABI cloud mask at each pixel.

The ADP also expects the Level 1b processing to flag any pixels with missing geolocation or viewing geometry information.

The ADP does check for conditions where the ADP cannot be performed and generates quality control flags for snow/ice pixel, pixels with saturated channels; pixels missed geolocation or viewing geometry information.

## 5.6. Algorithm Validation

For pre-launch validation, ADP algorithm will be extensively validated by using MODIS RGB images, MODIS aerosol product and Vertical Feature Mask from CALIPSO. The new analysis in the development to validate the ADP using AERONET and IMPROVE data will be presented in the next release of the ATBD as well as the ADP validation report. For post-launch validation, besides above-mentioned approach, field campaigns will also be carried out. Details on Algorithm Validation are given separately in the ABI ADP algorithm testing and validation plan document.

# 6. ASSUMPTIONS AND LIMITATIONS

The following assumptions have been made in the current algorithm:

- Calibrated and geo-located radiances in ABI channels as required by ABI ADP algorithm as shown in Table 2 are available;
- ABI cloud mask is available and adequate for the purpose of DP algorithm
- All the ancillary data are available.

Limitations applying to current algorithm are:

- Only for daytime
- Smoke detection over land is limited to dark surface

- Not optimal for optically thin smoke and dust
- No testing has been done to determine algorithm limitations if smoke and dust or other types of aerosols co-exist in the same pixel

## 6.2. Performance

The following assumptions are made in estimating the performance of ADP algorithm:

- smoke/dust mask from CALIPSO VFM represents the truth;
- visual separation of smoke, dust and clear pixels from MODIS RGB image introduces negligible error;
- Thresholds used in the current algorithm are tailored for MODIS channel specifications. Post –launch tuning of these thresholds will not affect the estimate of algorithm performance.
- In case of ABI sensor degradation, product production might squeeze but studies will be carried out prior to the launch on the extent of the effect any changes to instrument characteristics will have on product quality.

## *6.3.* Assumed Sensor Performance

ABI ADP algorithm assumes the sensor will meet its current specifications and produce calibrated quality radiance in the required channels (see Table 2). As shown in section 3.4.1., impacts from instrument noise and calibration error can be mitigated by adjusting threshold accordingly. However, ADP algorithm has low tolerance on missing channels. As discussed in above sections, ADP algorithm selects the optimal channels or combination of channels to best separate signal of smoke/dust from others. Therefore, missing any channel will definitely downgrade the performance of the algorithm and eventually leads to failure if crucial channels are missing. In addition, ADP algorithm will be dependent on the following instrumental characteristics.

- The spatial uniformity tests in ADP will be critically dependent on the amount of striping in the data.
- Errors in navigation from image to image will affect the performance of the temporal tests.

## 6.4. Pre-Planned Product Improvement

### 6.4.3. Improvement 1

Smoke detection over water is not optimal and will need improvements. We already improved the algorithm for the Version 5 release associated for the 100% delivery. Current algorithm has not been able to take advantage of temporal variability information that is unique for Geostationary Platform. We plan to utilize the rapid refresh rate of GOES_R ABI and improve the algorithm.

### 6.4.4. Improvement 2

The spectral screening thresholds are currently not a function of viewing and solar geometry. Testing will be carried out to understand the dependencies of some of the smoke/dust tests on viewing and solar geometries. Additional testing will also be done using simulated proxy data to determine ABI spectral thresholds and how robust these

spectral thresholds are under different scenarios. Based on these tests, algorithm could be improved.

### 6.4.5. Improvement 3

There are other algorithms based on spectral threshold tests that have been recently developed for SEVIRI. We will try to adapt those tests to improve smoke detection over water, dust detection over land and water, and also find a way to detect dust in the night time. Algorithm would have to be substantially altered for night time dust detection because visible channels will not be available.

### 6.4.6. Improvement 4

Validation of smoke/dust detection still remains a challenge at this stage. Besides the validation exercises that have already been completed, additional validations will be carried out. They include comparisons with the ground-based measurements and other satellite products. Validation with ground-based measurement will take advantage of measurements from aerosol sampler in IMPROVE network and Angstrom exponent information from AERONET for any indications of smoke/dust particle over some local and regional event. This, however, is not a direct comparison but an indirect subjective evaluation of smoke/dust detection product. For comparisons with other satellite products, Aerosol Index from OMI will be fully used to quantify the accuracy of smoke/dust products.

# 7. REFERENCES


Ackerman, S. A., Using the radiative temperature difference at 3.7 and 11mm to track dust outbreaks, *Remote Sensing of Environment*, **27**: (2) 129-133, 1989.

Ackerman, S. A., and K. I. Strabala, Satellite remote sensing of $H_2SO_4$ aerosol using the 8-12μm window region: Application to Mount Pinatubo. *J. Geophys. Res.*, **99**, 18,639-18,649, 1994.

Ackerman, S. A., Remote sensing aerosols using satellite infrared observations. *J. Geophys., Res.*, **102**, 17069–17079, 1997.

Ackerman, Steven A.; Strabala, Kathleen I.; Menzel, W. Paul; Frey, Richard A.; Moeller, Christopher C. and Gumley, Liam E., Discriminating clear sky from clouds with MODIS, *J. Geophys. Res.*, **103**, 32,141-32,157, 1998.

Ackerman, S. A., R. E. Holz, R. Frey, E. W. Eloranta, B. Maddux, and M. McGill, Cloud Detection with MODIS: Part II Validation. Accepted with revision to *J. Tech.*, 2008.

Barton, I. J., A. J. Prata, I. G. Watterson and S. A. Young, Identification of the Mount Hudson volcanic cloud over SE Australia. *Geophy. Res. Lett.*, **19**(12), June 19, 1992, 1211-1214, 1992.

Bohren, C. F. and D. R. Huffman, "Absorption and scattering of light by small particles", Wiley, New York, 1983.

Darmenovm A. and I. N. Sokolik, Identifying the regional thermal-IR radiative signature of mineral dust with MODIS, *Geophy. Res. Lett.*, **32**, doi:10.1029/2005GL023092, 2005.

Dubovik, O., Holben, B., Eck, T., Smirnov, A., Kaufman, Y., King, M., Tanré , D. and Slutsker, I., Variability of absorption and optical properties of key aerosol types observed in worldwide locations, *J. of Atmos. Sci.*, **59**, 590–608, 2002.

Dunion, J.P. and Velden, C.S., The Impact of the Saharan Air Layer on Atlantic Tropical Cyclone Activity, *Bulletin of the American Meteorological Society*, **90**, 353–365, 2004.

Evan, A. T., A. K. Heidinger, and M. J. Pavolonis, Development of a new over–water advanced very high resolution radiometer dust detection algorithm, *Int. J. Remote Sens*, **27**(18), 3903-3924, 2006.

Frey, R. A., S. A. Ackerman, Y. Liu, K. I. Strabala, H. Zhang, J. R. Key, and X. Wang, Cloud detection with MODIS, Part I: Improvements in the MODIS cloud mask for collection 5. *Journal of Atmospheric and Wateric Technology*, **25**, 7, 1057-1072, 2008.

Hansen, M., R. DeFries, J.R.G. Townshend, and R. Sohlberg, UMD Global Land Cover Classification, 1 Kilometer, 1.0, Department of Geography, University of Maryland, College Park, Maryland, 1981-1994, 1998.

IPCC, *Climate Change 2007*: The Physical Science Basis, Cambridge Univ. Press, New York, 996pp, 2007.

Kaufman, Y. J., et al., Operational remote sensing of tropospheric aerosol over land from EOS moderate resolution imaging spectroradiometer, *J. Geophys. Res.*, **102**, 16,971-16,988, 1997.

King, M. D., Menzel, W. Paul, Y. Kaufmann, Didier T., B.-C. Gao, S. Platnick, S. Ackerman, L. Remer, R. Pincus, and P. A. Hubanks, Cloud and aerosol properties,

precipitable water, and profiles of temperature and water vapor from MODIS. *IEEE Transactions on Geoscience and Remote Sensing*, **41**, 442-458, 2003.

Legrand, M., G. Cautenet, and J.-C. Buriez, Thermal impact of Saharan dust over land, Part II: application to satellite IR remote sensing, *J. Appl. Meteorol.*, **31**, 181-193, 1992.

Legrand, M., A. Plana-Fattori, and C. N'Doume, Satellite detection of dust using IR imagery of Meteosat 1. Infrared difference dust index, *J. Geophys. Res.*, **106**, 18,251-18,274, 2001.

Platnick, S., M. King, S. A. Ackerman, P. W. Menzel, B. A. Baum, J. C. Riédi, R. A. Frey, The MODIS Cloud Products: Algorithms and Examples from Terra, *IEEE Transactions on Geoscience and Remote Sensing*, **41**, 459-???, 2003

Prata, A. J., Observations of volcanic ash clouds in the 10-12-MU-M window using AVHRR/2 data. *International Journal of Remote Sensing* **10**(4-5), 751-761, 1989.

Rember, L., Y. J. Kaufman, D. Tanré, D., S. Mattoo, D. A. Chu, J. V. Martins, R-R. Li, C. Ichoku, R. C. Levy, R. G. Kleidman, T. F. Eck, E. Vermote, and B. N. Holben, The MODIS aerosol algorithm, products, and validation. *J. Atmos. Sci.*, **62**, 947–973, 2005.

Tanre, D., and M. Legrand, On the Satellite Retrieval of Saharan Dust Optical Thickness Over Land: Two Different Approaches, *J. Geophys. Res.*, **96**, 5221–5227, 1991.

Verge-Depre, G., M. Legrand, C. Moulin, A. Alias, and P. Francois, Improvement of the detection of desert dust over the Sahel using METEOSAT IR imagery, *Ann. Geophys.*, **24**, 2065-2073, 2006.

# Appendix 1: Common Ancillary Data Sets

## 1. LAND_MASK_NASA_1KM

### a. Data description

**Description**: Global 1km land/water used for MODIS collection 5
**Filename**: lw_geo_2001001_v03m.nc
**Origin**: Created by SSEC/CIMSS based on NASA MODIS collection 5
**Size**: 890 MB.
**Static/Dynamic**: Static

### b. Interpolation description

The closest point is used for each satellite pixel:

1) Given ancillary grid of large size than satellite grid
2) In Latitude / Longitude space, use the ancillary data closest to the satellite pixel.

## 2. MDS_L2_CLD_MASK_FILE

### a. Data description

**Description**: MODIS L2 cloud mask 1km
**Filename**: MOD35_L2.AYYYYDDD.HHMM.005.yyyydddhhmmss.nc /

MYD35_L2.AYYYYDDD.HHMM.005.yyyydddhhmmss.nc.
Where,
MOD35_L2/ MYD35_L2 – Level 2 Cloud Mask from TERRA (MOD) /
AQUA (MYD)
A – Nothing to do here
YYYYDDD – 4 digit year plus 3 digit of Julian day
HHMM – 2 digit of hour and 2 digit of minutes in GMT
005 – Processing system version
yyyydddhhmmss – processing date/time

**Origin**: NASA DAAC
**Size**: 45 MB
**Static/Dynamic**: Dynamic

### *b. Interpolation description*

The closest point is used for each satellite pixel:

In Latitude / Longitude space, use the ancillary data closest to the satellite pixel.

## *3. SNOW_MASK_IMS_SSMI*

### a. *Data description*

**Description**: Snow/Ice mask, IMS – Northern Hemisphere, SSM/I – Southern Hemisphere
4km resolution – the 25 km SSM/I has been oversampled to 4km
**Filename**: snow_map_4km_YYMMDD.nc
**Origin**: CIMSS/SSEC
**Size**: 39 MB.
**Static/Dynamic**: Dynamic

### b. *Interpolation description*

The closest point is used for each satellite pixel:

1) Given ancillary grid of large size than satellite grid
2) In Latitude / Longitude space, use the ancillary data closest to the satellite pixel.